



**HAL**  
open science

# Bioinspired pH-sensitive riboflavin controlled-release alkaline hydrogels based on blue crab chitosan: Study of the effect of polymer characteristics

Marwa Hamdi, Rim Nasri, S.M. Li, Moncef Nasri

## ► To cite this version:

Marwa Hamdi, Rim Nasri, S.M. Li, Moncef Nasri. Bioinspired pH-sensitive riboflavin controlled-release alkaline hydrogels based on blue crab chitosan: Study of the effect of polymer characteristics. *International Journal of Biological Macromolecules*, 2020, 152, pp.1252-1264. 10.1016/j.ijbiomac.2019.10.222 . hal-03790215

**HAL Id: hal-03790215**

**<https://hal.umontpellier.fr/hal-03790215v1>**

Submitted on 5 Oct 2022

**HAL** is a multi-disciplinary open access archive for the deposit and dissemination of scientific research documents, whether they are published or not. The documents may come from teaching and research institutions in France or abroad, or from public or private research centers.

L'archive ouverte pluridisciplinaire **HAL**, est destinée au dépôt et à la diffusion de documents scientifiques de niveau recherche, publiés ou non, émanant des établissements d'enseignement et de recherche français ou étrangers, des laboratoires publics ou privés.

1  
2  
3  
4 1 **Bioinspired pH-sensitive Riboflavin controlled-release alkaline**  
5  
6 2 **hydrogels based on blue crab chitosan: Study of the effect of wall**  
7  
8  
9 3 **polymer characteristics.**  
10  
11  
12

13 4 Marwa Hamdi <sup>a\*</sup>, Rim Nasri <sup>a,b</sup>, Suming Li <sup>c</sup>, Moncef Nasri <sup>a</sup>  
14

15 <sup>a</sup> Laboratory of Enzyme Engineering and Microbiology, University of Sfax, National Engineering School of Sfax,  
16 3038 Sfax, Tunisia.  
17 6

18  
19  
20 7 <sup>b</sup> Higher Institute of Biotechnology of Monastir, University of Monastir, Monastir, Tunisia.  
21  
22  
23

24 8 <sup>c</sup> European Institute of Membranes, UMR CNRS 5635, University of Montpellier, Place Eugene Bataillon, 34095  
25 Montpellier Cedex 5, France.  
26 9  
27  
28

29  
30  
31 11 \* **Corresponding author:** Marwa Hamdi, Laboratory of Enzyme Engineering and  
32  
33  
34 12 Microbiology, University of Sfax, National Engineering School of Sfax, B.P. 1173, 3038 Sfax,  
35  
36 13 Tunisia. **Tel:** 216 25740373 / 216 54186612; **E-mail:** [marwahamdi50@yahoo.fr](mailto:marwahamdi50@yahoo.fr).  
37  
38  
39  
40  
41  
42  
43  
44  
45  
46  
47  
48  
49  
50  
51  
52  
53  
54  
55  
56  
57  
58  
59

60  
61  
62 14 **Abstract**  
63

64  
65 15 Recently, the application of natural biocompatible polymeric hydrogels for the  
66  
67 16 conception of drug delivery matrices has attracted widespread interest. Thus, in the present  
68  
69 17 study, riboflavin pH-sensitive drug delivery hydrogels were developed based on blue crab  
70  
71 18 chitosan (Cs), via direct dissolution in alkali/urea aqueous solution at low temperatures. First,  
72  
73 19 the effect of Cs characteristics in terms of acetylation degree (AD) and molecular weight (Mw)  
74  
75 20 on the structural, mechanical, thermal, swelling and *in vitro* biodegradation of Cs-based  
76  
77 21 hydrogels were studied. Data from overall analysis revealed that Cs with low AD and high Mw  
78  
79 22 exhibited improved mechanical properties, as evidenced by the compressive and rheological  
80  
81 23 behaviors tests, thermal resistance, swelling behavior and *in vitro* degradation kinetics.  
82  
83 24 However, hydrogels pore sizes were reduced with the AD decrease and Mw increase.  
84  
85 25 Additionally, hydrogels in PBS (pH 5.5) underwent quicker degradation, compared to those  
86  
87 26 immersed in PBS (pH 7.4). In the drug delivery model, the kinetics of Riboflavin release,  
88  
89 27 through the Cs-based hydrogels were monitored. The Riboflavin release exhibited a typical tri-  
90  
91 28 phasic deliverance pattern, with significantly higher released amounts in more acidic systems.  
92  
93 29 Therefore, drug encapsulation within the conceived pH-sensitive Cs-based hydrogels could  
94  
95 30 provide suitable and promoting microenvironment for drugs delivery.  
96  
97  
98  
99  
100  
101  
102  
103  
104

105 33 **Keywords:** Hydrogels; Acetylation degree and Molecular weight; Drug controlled-  
106  
107 34 release.  
108  
109  
110  
111  
112  
113  
114  
115  
116  
117  
118

119  
120  
121 **37 1. Introduction**

122  
123 38 Hydrogels are three-dimensional hydrophilic polymeric networks with the ability to  
124  
125 39 absorb large amounts of water or biological fluids [1-2]. Because of their high-water content,  
126  
127 40 porosity and soft consistency, they closely simulate natural living tissues, more than any other  
128  
129 41 class of synthetic biomaterials and thus open up many possibilities for applications in  
130  
131 42 biomedical fields [3-5]. Physical hydrogels are distinguished from chemical hydrogels. The  
132  
133 43 network of physical hydrogels is maintained through weak bonds (hydrophobic, hydrogen,  
134  
135 44 ionic) that are not permanent because they are disconnected continuously depending on the  
136  
137 45 medium (pH, temperature, ionic strength). The chemical hydrogels, however, have a network  
138  
139 46 which is maintained by covalent crosslinks providing them a permanent character [6-7].

140  
141  
142 47 The high porosity that characterizes hydrogels can easily be adjusted by controlling the  
143  
144 48 density of the crosslinks in their matrix and their affinity to water. Moreover, their porous  
145  
146 49 structure allows to controllably loaded and released drugs [8-9]. The benefits of hydrogels for  
147  
148 50 drug delivery applications include the possibility of controlled and sustained release, which  
149  
150 51 permits a high local concentration of an active pharmaceutical ingredient (drug) to be  
151  
152 52 maintained over a long period of time. The drug can be loaded into a hydrogel, and then released  
153  
154 53 by several mechanisms: controlled release, controlled swelling, chemically controlled release  
155  
156 54 and environmental release [10].

157  
158  
159 55 The rate of release can be managed by modifying some factors such as polymer  
160  
161 56 concentration, crosslinking density, and water content. Some «smart» hydrogels have the ability  
162  
163 57 to respond to external stimuli such as pH, temperature, ionic strength, etc., making them  
164  
165 58 excellent site-specific active ingredient in delivery matrices for diseases prevention and  
166  
167 59 treatment [11-12].

170  
171 60 Hydrogels are of great interest for other biomedical applications because of the ability to  
172  
173 61 control their swelling, mechanical properties, chemical and physical structures, crosslinking

178  
179  
180 62 density and porosity. Therefore, hydrogels are frequently used in tissue engineering for cell  
181  
182 63 encapsulation or drug delivery, but as well as wound dressings, bioadhesives and biosensors  
183  
184  
185 64 [13-14]. In fact, hydrogels can serve as templates for directing cell behavior and promoting cell  
186  
187 65 organization. In addition, the biocompatibility of hydrogels has generated a lot of interest in  
188  
189 66 hygiene products, implants and soft contact lenses [15-16].

190  
191 67 Advantageously, chitosan can be used in the preparation of hydrogels which serve as a  
192  
193 68 matrix for the incorporation of active agents [17-19]. As part of this research, chitosan obtained  
194  
195 69 by partial deacetylation of chitin was chosen. Chitosan-based hydrogels have shown important  
196  
197 70 advantages in terms of drug delivery, as they allow site-specific and / or time-controlled  
198  
199 71 administration for small and large drugs [17,20]. They offer, furthermore, many benefits, such  
200  
201  
202 72 as improving biosecurity and drug efficacy. Chitosan hydrogels can provide targeted delivery  
203  
204 73 and improved stability of therapeutic agents against physiological degradation [17].

205  
206 74 To the best of our knowledge, there is a lack of information in literature regarding the  
207  
208 75 effect of acetylation degree and molecular weight on chitosan-based hydrogels, although  
209  
210 76 several reports describe their developpement and application in particularly the biomedical  
211  
212 77 field. Therefore, the objective of this work was the conception of high strength hydrogels based  
213  
214 78 on chitosans with different acetylation degrees and molecular weights, to assess the effects of  
215  
216 79 these two structural parameters on the properties of the resulting hydrogels. Subsequently, the  
217  
218  
219 80 selected hydrogel was applied for controlled release of Riboflavin with very interesting  
220  
221 81 biological potential, as drug model.

## 222 223 82 **2. Materials and methods**

### 224 225 226 83 **2.1. Materials**

227  
228 84 Riboflavin was purchased from LOBA CHEMIE (India) and the other used chemical  
229  
230 85 reagents from commercial sources were of analytical grade and employed without further  
231  
232 86 purifications.  
233  
234  
235  
236



## 2.2. Chitosans preparation and purification

Chitosans (Cs) from blue crab *Portunus segnis* shells were prepared in our laboratory, as described in our previous study [21]. Briefly, Cs with different AD were obtained through chitin N-deacetylation with NaOH 12.5 M at a w/v ratio of 1/10 at 140 °C, for 2, 3 and 5 h and produced Cs were named Cs I, Cs II and Cs III. After filtration, Cs was washed to neutrality and then dried for 12 h at 50 °C. Based on the nuclear magnetic resonance (<sup>13</sup>C NMR) analysis, ADs of 17%, 13% and 8% were reached for Cs I, Cs II and Cs III, respectively. Further, Cs were characterized by size exclusion chromatography (SEC-HPLC) and average molecular weights (Mw) of 125 600, 118 900 and 115 000 g mol<sup>-1</sup> were obtained for CsI, CsII and CsIII, respectively.

To generate Cs with different Mw, Cs, at different ADs, were hydrolyzed with Cellulase (10 U/g chitosan) in 0.5 N acetate-bicarbonate buffer (pH 5.2) at 55 °C, for 1 and 3 h, as described by Chang *et al.* [22] with slide modifications. The Cs obtained are lyophilized and analyzed to study the evolution of their molecular mass. The respective Mw were reported in

### Table S1.

Subsequently, Cs were purified according to the method described by Qian and Glanville [23]. Thus, crude Cs (6 g) was dissolved in 600 ml of HCl 0.1 M under stirring overnight at a temperature of 40 °C. The acidic solution was vacuum filtered to remove insoluble particles. Cs was then precipitated with NaOH 0.5 M under continuous stirring until approximately pH 8.5. Thereafter, 6 ml of 10% (w/v) sodium dodecyl sulfate (SDS) was added to the suspension and the mixture was heated at 95 °C for 5 min. After cooling at room temperature, the pH was adjusted to 10.0 with 0.5 M NaOH. The mixture was vacuum filtered and the hydrated Cs was washed 5 times with 600 ml of deionized water at 40 °C. A solution of barium chloride was used to confirm the absence of residual SDS in the filtrate. Finally, the obtained purified Cs were lyophilized, milled to powder and then sieved.

### 2.3. Conception of blue crab chitosan-based hydrogels

Hydrogels were prepared based on the freezing/thawing approach described by Duan *et al.* [5]. Briefly, Cs, derived from the action of Cellulase, were dissolved in an alkaline solution, widely used for the dissolution of cellulose and chitin, consisting of 4.5 wt. % LiOH, 7.5 wt. % KOH and 8.5 wt. % urea. Then, the reaction mixtures were maintained at -30 °C until complete freezing, followed by a thawing step at 20 °C under vigorous agitation, until a clear and transparent solution of Cs was obtained. After removal of air bubbles by centrifugation at 5000 ×g for 15 min at 4 °C, the prepared solutions were maintained at 60 °C for 1 h (solvent evaporation technique), promoting the formation of Cs physical gels. After exhaustive washing with Milli-Q water, to remove the residual alkali/urea solution, prepared hydrogels were immersed in an ethanol solution (100%) for 3 days to improve the resistance of the gels [24].

Foremost, Cs-based hydrogels with different AD and Mw were prepared at a concentration of 3% (w/v) [24], to study the effect of these two parameters on the structural, mechanical and rheological features of elaborated hydrogels. The corresponding code to each hydrogel was recorded in **Table S2**. Subsequently, an optimization of the ideal concentration for the formation of Cs-based hydrogels was performed. Accordingly, different concentrations were used, namely 1%, 2%, 3%, 4% and 5% of Cs, and the obtained hydrogels were characterized.

### 2.4. Blue crab chitosan rheological behavior in the alkali/urea aqueous solution

To study the stability of the Cs in alkali/urea system, hydrogels (15 mm of diameter × 1 mm of thickness) rheological and gelation behaviors were investigated with dynamic viscoelastic measurements. For all the experiments, a rheometer apparatus (Physica MCR, Anton Paar, GmbH, France) equipped with a plate-plate measuring geometry (25 mm diameter, 0.1 mm gap) was used. Oscillatory measurements of the storage modulus ( $G'$ ) and loss modulus ( $G''$ ) were carried out under a strain sweep from 0.1% to 1000% at 37 °C with a frequency of 1



355  
356  
357 137 Hz. Thermo-viscoelasticity properties in a ramp temperature from 20 to 80 °C was investigated,  
358  
359 138 under constant frequency (1 Hz) and strain (1%), at a heating rate of 2 °C/min. A solvent trap  
360  
361  
362 139 was applied to prevent water evaporation when heating. The data were analyzed with Rheoplus  
363  
364 140 software from Anton Paar.

## 366 141 **2.5. Analytical methods**

### 368 142 **2.5.1. Hydrogels microstructure**

369  
370  
371 143 The cross-section of Cs-based hydrogels was studied using scanning electron microscopy  
372  
373 144 SEM (Hitachi S4800), at an angle of 90° to the surface, at different magnifications. Prior to  
374  
375 145 imaging their cross-section, hydrogel samples were lyophilized, sectioned and fixed on the  
376  
377 146 SEM support using double side adhesive tape, and observed up to a 2000 x magnification, under  
378  
379 147 an accelerating voltage of 2.0 kV and an absolute pressure of 60 Pa, after being sputter coated  
380  
381 148 with a 5 nm thick gold.

### 384 149 **2.5.2. Moisture content of Cs-based hydrogels**

385  
386 150 The water content was determined according to the methods described by AOAC (2000)  
387  
388 151 [25]. The water content of the elaborated hydrogels was measured, in triplicate, by drying about  
389  
390 152 100 mg of each sample in an oven at 105 °C until the dry weight of the sample was reached  
391  
392  
393 153 (constant weight). Weights before and after drying were measured. The moisture content of  
394  
395 154 hydrogels was determined by measuring the mass loss of each film in triplicate and expressed  
396  
397 155 as follows:

$$400 \quad 156 \quad MC (\%) = \frac{W_0 - W_1}{W_0} \times 100$$

403 157 where  $W_0$  and  $W_1$  are the respective masses (g) of hydrogels before and after drying at 105 °C.

### 405 158 **2.5.3. Swelling rate of hydrogels**

406  
407 159 The swelling test was performed on pieces of hydrogels with masses of 20-30 mg. The  
408  
409  
410 160 samples were immersed in phosphate-buffered saline (PBS) at 37 °C and after 24 h of

414  
415  
416 161 incubation, the samples were removed, oven-dried and the masses were measured again [26].

417  
418 162 The swelling rate (SR), repeated three times, was calculated as follows:

419  
420  
421 163 
$$SR (\%) = \frac{M_s - M_d}{M_d} \times 100$$

422  
423  
424 164 where SR is the swelling rate (%),  $M_d$  is the mass (g) of the oven-dried hydrogel and  $M_s$  is the  
425  
426 165 mass (g) of the swollen hydrogel.

#### 427 428 429 166 **2.5.4. Infrared spectroscopy analyses**

430  
431 167 The prepared Cs-based hydrogels FT-IR analysis was performed by means of a  
432  
433 168 spectrometer (Agilent Technologies, Carry630 series) with an attenuated reflection accessory  
434  
435 169 (ATR) containing a diamond/ZnSe crystal, at room temperature (25 °C). Spectra were recorded  
436  
437  
438 170 in the spectral range frequencies of 650-4000  $\text{cm}^{-1}$ , with 32 scans of interferograms and a  
439  
440 171 resolution of 4  $\text{cm}^{-1}$ . Prior to analysis, FT-IR spectrometer was calibrated via a background  
441  
442 172 spectrum recorded from the clean and empty diamond for each spectrum. Data analysis and  
443  
444 173 treatment were carried out using the OMNIC Spectra software (ThermoFisher Scientific).

#### 445 446 447 174 **2.5.5. X-ray diffraction studies**

448  
449 175 To further investigate the structural characteristics of the prepared hydrogels, XRD  
450  
451 176 patterns were recorded using an X-ray diffractometer (D8, Advance Bruker XRD  
452  
453 177 diffractometer, Germany). Ni-filtered Cu  $K\alpha$  radiation ( $k = 1.5406 \text{ \AA}$ ) was used to record the  
454  
455 178 X-ray patterns. The relative intensity was recorded in the scattering range  $2\theta$  of 5–50° with a  
456  
457 179 step size of 0.02° and a counting time of 5 s/step, with an error of  $\pm 1^\circ$ .

#### 458 459 460 180 **2.5.6. Thermal properties of blue crab chitosan-based hydrogels**

461  
462 181 Thermogravimetric analysis (TGA Q500 High Resolution, TA Instruments), operating  
463  
464 182 under nitrogen flow, was used to study the thermal stability of Cs-based hydrogels. The mass  
465  
466 183 change of a sample as a function of temperature augmentation is the basis of TGA, and the  
467  
468  
469 184 progressive change in mass (%) as function of temperature, is recorded. Cs-based hydrogels,

473  
474  
475 185 initially about 4 mg, were heated from 25 to 700 °C at a heating rate of 20 °C/min and constantly  
476  
477 186 measured with an accuracy of 0.01 mg. Cs-based hydrogel thermograms were subsequently  
478  
479  
480 187 analyzed using TA Universal V4.5A software.

### 482 188 **2.5.7. Evaluation of hydrogels mechanical properties**

484 189 Hydrogel compression tests were carried out using the DMA50 (Dynamic Mechanical  
485  
486  
487 190 Analyzer) universal testing machine (Metravib, Brand of ACOEM, France) at a temperature of  
488  
489 191 25 °C and a compression speed of 1 mm/min. Samples were compressed at 10%, 20%, 30%,  
490  
491 192 40%, 50% and 60%, and then reverted at the same speed of 1 mm/min, to obtain the stress-  
492  
493 193 strain curves for gels' compression-recovery. The dimensions of the hydrogel specimens  
494  
495 194 (parallelepiped) for compression tests were 10 mm × 5 mm × 5 mm (based on the apparatus  
496  
497 195 requirements). The stress-strain curve hysteresis was recorded and treated by the instrument  
498  
499 196 software.

### 502 197 **2.5.8. Hydrogels *in vitro* degradation test**

504 198 Cs-based hydrogels *in vitro* biodegradation study was monitored through the gravimetric  
505  
506 199 method described by Qu *et al.* [27]. Briefly, hydrogels (approximately 100 mg) were  
507  
508 200 immersed in 10 ml of phosphate buffer saline (PBS) at pH 7.4 (physiological microenvironment  
509  
510  
511 201 simulation) and pH 5.5 (acidic microenvironment), at 37 °C and under gentle shaking  
512  
513 202 (approximately 100 rpm). Thereafter, hydrogel samples were removed, at each desired  
514  
515 203 interval time, washed with Milli-Q water to remove the excess of salinity, oven-dried for 48 h  
516  
517 204 at 60 °C and then weighed. The remaining weight of hydrogels (%) was calculated based on the  
518  
519 205 following equation:

$$\text{Remaining weight ratio (\%)} = \frac{M_t}{M_i} \times 100$$

523 206  
524  
525 207 where  $M_t$  is the remaining hydrogels dry weight after degradation at each selected time interval  
526  
527 208 and  $M_i$  is the initial hydrogels dry weight.

## 2.6. *In vitro* riboflavin loading and release kinetics

The amount of riboflavin incorporated in hydrogels was studied. Briefly, wet Cs-based hydrogel (30 mg) were suspended in 10 ml of riboflavin solution (1-5 g/l) in dark at 5 °C for 48 h. The riboflavin entrapment efficiency and loading capacity by the hydrogels were determined considering the derivative thermogravimetric (DTG) thermograms [28], by subtracting the amount of riboflavin in the supernatant from the total amount applied [24]:

$$\text{Riboflavin loading capacity (\%)} = \frac{\text{Mass of loaded riboflavin}}{\text{Mass of hydrogel samples}} \times 100$$

$$\text{Riboflavin entrapment efficiency (\%)} = \frac{\text{Mass of loaded riboflavin}}{\text{Mass of initial riboflavin}} \times 100$$

Regarding the riboflavin release studies, loaded hydrogel samples (30 mg) were subsequently incubated in 10 ml of aqueous HCl and NaCl (0.1 M) with different pH values (pH 2.0, 4.5 and 7.4) at 37 °C, with stirring. At each time interval, an aliquot of the supernatant (2.5 ml) was withdrawn and replaced by fresh medium at the same volume. The amount of released riboflavin was determined spectrophotometrically, considering the cumulative amount of riboflavin in each of the release system. The amount of riboflavin was estimated using a UV-visible spectrometer (Agilent Technologies, Carry 630 series) at 450 nm on the basis of a riboflavin calibration curve (**Data not shown**). All studies were performed in duplicate and the average values were reported.

## 2.7. Statistical analysis

Statistical analyses were performed with SPSS ver. 17.0, professional edition (SPSS, Inc., Chicago, IL, USA) using ANOVA analysis at a p-value < 0.05. A standard deviation at the 95% confidence level was used to compare all parameters analyzed for the different hydrogels. All assessments were repeated three times and average values with standard deviation errors were reported.

### 3. Results and Discussion

#### 3.1. Microstructure analysis of Cs-based hydrogels

Since understanding biomaterials functional properties is based on their structure knowledge, the examination of Cs-based hydrogels microstructure, reflecting polymer and molecules interactions, is required [29].

SEM images showing the pore microstructure (cross section) of Cs-based hydrogels, with different AD and Mw, are displayed in **Fig. 1**. The pore size of the prepared hydrogels changed in the range of 1 ~ 6  $\mu\text{m}$  and became bigger and bigger as the Cs AD increased, with more compact distribution. For example, pore size values of ~ 1  $\mu\text{m}$  for CsIII-0 based hydrogel (**Fig. 1G**), 2  $\mu\text{m}$  for CsII-0 based hydrogel (**Fig. 1D**) and 3  $\mu\text{m}$  for CsI-0 based hydrogel (**Fig. 1A**) were reached, suggesting that lower AD allowed the preparation of a more well-organized network structure, which could contribute to mechanical support [30].

It was found likewise that the hydrogel pore size had the tendency to decrease with the increase of Cs Mw. Indeed, the pore size (approximately 4  $\mu\text{m}$ ; **Fig. 1I**) of CsIII-3 based hydrogel, showing a microstructure, filled with larger interconnected pores, was about twice of that for CsIII-1 based hydrogel (approximately 2  $\mu\text{m}$ ; **Fig. 1H**), which could lead to modulations in Cs-based hydrogels swelling and drug release behaviors [17].

In another aspect, overall Cs-based hydrogels, regardless Cs AD and Mw, as shown in **Fig. 1**, the formed hydrogels network revealed a uniformly distributed porous three-dimensional architecture, with, to variable extend, a roughness matrix surface. The pores interconnected in a recurrent style inside the hydrogels network affords a suitable medium flow and drug transport channels, being therefore appropriate for drug delivery [26,31].

#### 3.2. Hydrogels moisture content determination

Moisture content (MC) of Cs-based hydrogels, reported in **Table 1**, revealed that values decreased with the decrease of the AD, reaching 82%, 81% and 79%, for CsI-0 (AD=17%),

650  
651  
652 257 CsII-0 (AD=13%) and CsIII-0 (AD=8%) based hydrogels, respectively ( $p<0.05$ ). however,  
653  
654 258 considering Cs Mw, MC values were found to be strengthened with the decrease of Cs Mw.  
655  
656 259 Indeed, regarding an AD of 8% (CsIII), hydrogels MC rates of 79.90%, 80.26% and 81.83%  
657  
658 260 were reached with respective Mws of 115 kDa (CsIII-0), 78.43 kDa (CsIII-1) and 16.04 kDa  
659  
660 261 (CsIII-3), probably due a decrease of crosslinking density [5]. In fact, hydrogels are systems  
661  
662 262 known for their remarkable water-holding capacity during their preparation, and the water  
663  
664 263 content is one of the most features that distinguishes hydrogels from other biomaterials. Their  
665  
666 264 water-rich structure facilitates, indeed, the transport of nutrients and molecules between the  
667  
668 265 external environment and the hydrogel, which allows to mimic the function of cells in the body  
669  
670 266 [9].  
671  
672  
673

674 267 Consequently, it could be proposed that the increase of CS MW, besides the decrease of  
675  
676 268 its AD, as well as Cs-based hydrogels soaking in ethanol solution (100%), allowed the decrease  
677  
678 269 in Cs-based hydrogels water content, and thereby, reducing pore sizes [24], which was  
679  
680 270 consistent with SEM data. This finding seems to be beneficial for Cs-based hydrogels  
681  
682 271 mechanical properties enhancement.  
683  
684

### 685 272 **3.3. Evaluation of Cs-based hydrogels swelling properties**

686

687 273 As an absorbent matrix, the degree of swelling of a hydrogel is a key parameter that is  
688  
689 274 closely related to the ability of hydrogels to release active ingredients [32]. Swelling is defined  
690  
691 275 as a continuous transition process from the solvent-free glassy state or partially rubbery state to  
692  
693 276 a relaxed rubbery solvent containing state. The solvent infiltration and the elastic contraction  
694  
695 277 from the network strain, as two opposite forces, create a skirmish in the swelling process, which  
696  
697 278 reaches the equilibrium, when they reach a dynamic balance [33]. In this context, the effect of  
698  
699 279 Cs AD and Mw on Cs-based hydrogels swelling ratio (SR) was studied and results are recorded  
700  
701 280 in **Table 1**.  
702  
703  
704  
705  
706  
707  
790

709  
710  
711 281 Results display that Cs-based hydrogels water absorption capacity was found to be  
712  
713 282 dependent to the Cs AD and Mw. Indeed, SR values increased with the decrease of Cs AD as  
714  
715  
716 283 well as the decrease in its Mw. For example, hydrogels developed with CsI (CsI-0; AD=17%)  
717  
718 284 exhibited SR value of  $13.59 \pm 0.45$  g/g, compared to CsIII-0 based hydrogel, prepared with lower  
719  
720 285 AD Cs (CsIII-0; AD=8%), with SR exceeding 18 g/g (**Table 1**). Moreover, regarding CsIII-  
721  
722 286 based hydrogel, respective SR values of more than 18 g/g, 22 g/g and 26 g/g were reached with  
723  
724 287 hydrogels prepared with GCsIII-0 (115 kDa), GCsIII-1 (78.43 kDa) and CsIII-3 (16.04 kDa).  
725

726 288 It is well known that the swelling properties of hydrogels depend on the hydrophilic  
727  
728 289 nature of polymeric chains and the nature of bonds inside the matrix structure. Thus, it is  
729  
730 290 possible to deduce that the decrease of Cs AD, and thereby, the increase of the  $-NH_2$  groups  
731  
732 291 number, allowed the improvement of the hydrophilicity of the elaborated hydrogels, favoring  
733  
734 292 their interaction with water molecules [34,35]. In addition to the polarity of the hydrogels, the  
735  
736 293 degree of crosslinking and hydrogels porosity were found to well correlate with the ability of  
737  
738 294 Cs-based hydrogels to absorb water [12,27].  
739  
740  
741

### 742 295 **3.4. Hydrogels spectroscopic characterizations**

#### 743 744 296 **3.4.1. FT-IR analysis**

745  
746 297 The FT-IR spectra of Cs-based hydrogels were shown in **Fig. 2**. Compared to the polymer  
747  
748 298 powder [21], characteristic Cs absorption bands at  $3417\text{ cm}^{-1}$ ,  $1627\text{ cm}^{-1}$ ,  $1544\text{ cm}^{-1}$ ,  $1407\text{ cm}^{-1}$   
749  
750 299  $^{-1}$  and  $1020\text{-}1097\text{ cm}^{-1}$  linked to the  $-OH$ , amide I groups ( $-C=O$ ), amide II ( $-NH_2$ ),  $-CH$  and  
751  
752 300 glycoside rings, respectively, were noted to be rearranged. Indeed, the  $N-H$  peak in the FT-IR  
753  
754 301 spectra of the Cs-based hydrogels was found to be shifted significantly to higher wavenumbers  
755  
756 302 overlapping with the peak of the  $O-H$  stretching vibrations. The peak at  $3500\text{-}3200\text{ cm}^{-1}$   
757  
758 303 straitened, and revealed the tendency to break into several small peaks, demonstrating the  
759  
760 304 weakening of the inter- and intra-molecular hydrogen bonds and the occurrence of some  
761  
762 305 reactions on the two groups [34-39].  
763  
764  
765  
766  
826

768  
769  
770 306 The peak of the amide I group weakened remarkably and almost disappeared, indicating  
771  
772 307 that concentrated alkali has reacted with the acetyl amino group of Cs [38,39]. Moreover, new  
773  
774 308 stretch vibration absorption bonds appeared at about  $3264\text{ cm}^{-1}$ ,  $2500\text{ cm}^{-1}$  and  $785\text{ cm}^{-1}$ ,  
775  
776 309 indicating that the alkali/urea aqueous solvent affected the structure of Cs to some extent.  
777  
778  
779 310 Indeed, active hydroxyl group of Cs reacted with the concentrated alkali, leading thereby to the  
780  
781 311 destruction of the native hydrogen bonds of Cs effectively and making Cs highly swell or even  
782  
783 312 dissolve in the alkali solution.  
784

785 313 These findings confirmed further during the dissolution process, alkali not only reacts  
786  
787 314 with the hydroxyl group, but also with the acetyl amino group of Cs, leading to the weakening  
788  
789 315 of the amide I peak ascribed to acetyl amino group [40,41]. Moreover, The FT-IR spectra of all  
790  
791 316 Cs-based hydrogels are quite similar, regardless Cs AD and Mw, accounting for the stability of  
792  
793 317 Cs in the alkali/urea aqueous solution system [24, 42,43].  
794  
795

### 796 318 **3.4.2. XRD patterns study**

799 319 To further clarify the structural changes in the Cs matrix, during dissolution in the  
800  
801 320 alkali/urea aqueous system and gelling, and regarding the effects of Cs Mw and AD, XRD  
802  
803 321 patterns of Cs-based hydrogels were studied and compared to the polymer powder profiles (**Fig.**  
804  
805 322 **3**). X-diffractograms of Cs-based hydrogels revealed marked differences in the molecular state.  
806  
807 323 Indeed, diffraction peaks nearby  $13.1^\circ$  and  $21.3^\circ$ , attributed to (020) and (110) planes of Cs,  
808  
809 324 respectively, were detected, reflecting the semi-crystalline structure of Cs [21,44]. The major  
810  
811 325 peaks at  $2\theta = 37.7^\circ$ ,  $34.32^\circ$ ,  $32.4^\circ$  and  $28.9^\circ$  observed in the X-diffractograms could be  
812  
813 326 attributed to the alkali (LiOH) used for the dissolution of Cs [45].  
814  
815

816 327 As shown in **Fig. 3**, the Cs-based hydrogels displayed the characteristic diffraction  
817  
818 328 patterns of both Cs and alkali at the same time. However, the crystallinity of the physical Cs-  
819  
820 329 based hydrogels clearly diminished in comparison with that of Cs powder, where the above  
821  
822 330 mentioned initial characteristic peaks became broader and weaker, depending on Cs AD and  
823  
824  
825  
826



827  
828  
829 331 Mw. In fact, convenient with the SEM images, the crystallinity of Cs-based hydrogels decreased  
830  
831 332 with the increase of Cs AD (CsI-0 based hydrogel) and the decrease in its Mw (Cs-1 and Cs-3  
832  
833 based hydrogels), suggesting a transition from a crystalline structure to an amorphous state  
834  
835 during the dissolution and the gelling process [46,47]. This result strongly confirmed that Cs  
836  
837 solubility was related to its crystallinity.  
838  
839

840 336 With the aid of alkali solution and the freezing to -30 °C, water molecules diffuse in the  
841  
842 337 Cs macromolecular chain. The subsequent thawing and stirring steps during hydrogels  
843  
844 338 preparation process are beneficial for the dissolution of Cs, as the intra- and inter-molecular  
845  
846 339 hydrogen bonds of Cs would be broken during dissolution, leading to the loss of crystallinity  
847  
848 340 [48,49].  
849  
850

851 341 The dissolution of Cs in the alkali aqueous system begins at the amorphous side with a  
852  
853 342 loose structure at first, and afterwards reaches the crystal zone with a rather thicker construction  
854  
855 343 and low temperature. This exhibits a crucial role in the Cs crystalline configuration destruction  
856  
857 344 [26,50]. Meanwhile, overall findings proposed that the chemical structure of Cs was relatively  
858  
859 345 stable in the alkali/urea aqueous solution [5,24].  
860  
861

### 862 346 **3.5. Cs AD and Mw affected based hydrogels thermal properties**

863

864 347 Thermal stability/degradation behavior of Cs-based hydrogels, with respect to their AD  
865  
866 348 and Mw, was studied, and results in terms of TGA and derivate (DTG) thermograms, are shown  
867  
868 349 in **Supplementary data Fig. S1**. The thermal decomposition data in terms of the corresponding  
869  
870 350 degradation temperatures, the weight loss ( $\Delta w$ ) and the residue (**R**), were estimated (**Table 2**).  
871

872 351 Based on data from the obtained TGA thermograms, the thermal decomposition profiles  
873  
874 352 of the overall Cs-based hydrogels exhibited a similar weight loss process in the temperature  
875  
876 353 range of 20–800 °C, indicating the polymer pyrolysis, and characterized by three major phases  
877  
878 354 (**Supplementary data Fig. S1**), typical fingerprint of Cs thermal decomposition [32].  
879  
880  
881  
882  
883  
884

886  
887  
888 355 The first phase corresponded to a weight loss of 6% (CsIII-0 based hydrogel) to 19%  
889  
890 356 (CsI-3 based hydrogel), apparently resulted from evaporation of adsorbed water by Cs at a  
891  
892  
893 357 temperature (Td1) range from 28-46 °C to 129-158 °C, reaching its maximum mainly below  
894  
895 358 130 °C, expect for the CsIII-0 based hydrogel (133.54 °C). The different content of bound and  
896  
897 359 unbound water in the hydrogels could explain the observed difference in onset temperature [51].  
898  
899 360 Indeed, in line with data from the SEM analysis and results above mentioned, CsIII-0 based  
900  
901 361 hydrogel exhibited higher onset temperature as a result of more strongly bound water, related  
902  
903 362 to a more homogeneous network structure. However, less uniform network with macro-phase  
904  
905 363 separation like structure, observed in hydrogels based on CsI-3, was found to responsible of  
906  
907 364 more unbound water in the based hydrogel structure [28,48].  
908  
909

910 365 Considering the DTG curves, the temperature, at which the decomposition process was  
911  
912 366 the shrillest, was revealed by the weight loss peak (**Supplementary data Fig. S1**). In the range  
913  
914 367 the third phase of Cs-based hydrogels pyrolysis process (200-550 °C), where higher  $\Delta W$  were  
915  
916 368 reached, peaks located at temperatures of 268.81, 266.09 and 261.55 °C, were found for the  
917  
918 369 CsI-0, CsI-1 and CsI-3 based hydrogels, respectively, whereas those found at 279.71, 274.26  
919  
920 370 and 273.35 °C were related to the CsIII-0, CsIII-1 and CsIII-3 based hydrogels, respectively  
921  
922 371 (**Table 2**). Thus, polymers pyrolysis temperature differences are mainly assigned to the  
923  
924 372 macromolecular interaction, crystallinity index, or orientation. The TGA results proved that  
925  
926 373 CsIII-0 based hydrogel was reorganized in more well-ordered network structure, during the  
927  
928 374 dissolution in the alkali/urea system at low temperatures and the regeneration process in  
929  
930  
931 375 ethanol, ensuing a rather high crystallinity and more homogeneous architecture. Finally,  
932  
933 376 residual decomposition reactions leading to the total degradation of the Cs ring in the hydrogels  
934  
935 377 was found to be around 550 °C [52].  
936

937 378 Regarding the residual mass (R) of the prepared hydrogels, values were found to decrease  
938  
939 379 with the decrease of the Cs Mw and the increase of its AD, with values of 33.70% (CsI-0 based  
940  
941  
942  
943  
885

945  
946  
947 380 hydrogel), 30.59% (CsI-1 based hydrogel) and 29.88% (CsI-3 based hydrogel). Considering  
948  
949 381 CsII-based hydrogels, R values of 34.34%, 33.05% and 29.58% were reached for the CsII-0,  
950  
951 382 CsII-1 and CsII-3 based hydrogels, respectively. R values of 47.69%, 40.53% and 38.68% were  
952  
953  
954 383 noted for CsIII-0, CsIII-1 and CsIII-3 based hydrogels, respectively (**Table 2**). Accordingly, it  
955  
956 384 could be concluded that the thermal stability of the Cs-based hydrogels is positively correlated with  
957  
958 385 its AD and disproportionate to its Mw. Moreover, as discussed earlier, TGA findings confirmed  
959  
960 386 that the increased stability of the Cs-based hydrogels was due to increasing macromolecular  
961  
962 387 chains crosslinking [28,32].

### 963 964 965 388 **3.6. Hydrogels mechanical properties as affected by Cs structural parameters**

#### 966 967 389 **3.6.1. Rheological behavior**

968  
969 390 The rheological properties of Cs-based hydrogels, storage modulus ( $G'$ ) and loss modulus  
970  
971 391 ( $G''$ ), were shown as a function of strain at 37 °C (**Fig. 4A-C**). Independently of Cs AD or Mw,  
972  
973 392 Cs-based hydrogels displayed higher elastic behavior ( $G' > G''$ ) than the viscous behavior  
974  
975 393 ( $G' < G''$ ), suggesting a distinctive feature of a strong hydrogel.

976  
977  
978 394 Since the elasticity of the sample, defined as the stored energy due to the elastic  
979  
980 395 deformation, is reflected by the storage modulus  $G'$ , the higher the  $G'$  value is, the tougher  
981  
982 396 against distortion the hydrogel is [33]. **Fig. 4A-C** shows that for all the Cs-based hydrogel  
983  
984 397 samples, the moduli ( $G'$  and  $G''$ ) fluctuated slightly with deformation in the test strain range of  
985  
986 398 500%. Comparing the hydrogel samples, for CsIII-0 based hydrogel, the  $G'$  (more than 130  
987  
988 399 kPa) was found to be significantly higher than that of CsII-0 (more than 82 kPa) and CsI-0  
989  
990 400 (more than 35 kPa) based hydrogels. Additionally, for CsIII-1 ( $G'$  about 30 kPa) and CsIII-3  
991  
992 401 ( $G'$  more than 17 kPa) based hydrogels, the  $G'$  values were significantly lower than that of  
993  
994  
995 402 CsIII-0 based hydrogel ( $p < 0.05$ ). The same tendency was detected with the other hydrogels  
996  
997 403 based on CsII (AD of 13%) and GCsI (AD of 17%).

1004  
1005  
1006 404 Before hydrolysis,  $G'$  of Cs-based hydrogels, independently of Cs AD, was four times  
1007  
1008 405 more than the value of Cs-1 and Cs-3 based hydrogels, thus, the creation of a more stable  
1009  
1010 406 network, leading to a greater maximum storage modulus  $G'$ .

1012 407 This finding could be mainly assigned to the stronger interactions of Cs macromolecular  
1013  
1014 408 chains, with high average molecular weight, than medium and lower average molecular weights  
1015  
1016 409 Cs (Cs-1 and Cs-3, respectively). The formation of covalent bonds between the Cs and the  
1017  
1018 410 alkali/urea system, allowed thereby remarkably the enlargement of the strength of hydrogels  
1019  
1020 411 and the enhancement of their mechanical properties [5,27,33].

1023 412 Data of gradually decreasing storage modulus  $G'$  of the hydrogels, with the decrease of  
1024  
1025 413 Cs AD and the increase of the Mw, were consistent with the gradually increasing SR results  
1026  
1027 414 above described (**Table 1**), further, principally ascribed to the progressively hydrogels  
1028  
1029 415 crosslinking density diminishing [24,53].

1031 416 As displayed in **Fig. 4A-C**, it is likewise found that an increase in the deformation, more  
1032  
1033 417 than 500%, was associated with loss/viscous modulus  $G''$  enlargement and storage/elastic  
1034  
1035 418 modulus  $G'$  decline, as the network movement increased [54], demonstrating that at higher  
1036  
1037 419 strains elastic flow of the gel network decreased. However, unlike the  $G'$  profile, the gel-sol  
1038  
1039 420 transition strain value was found not significantly influenced with the Cs AD or Mw.

1041 421 In another aspect, there was found no remarkable difference of Cs-based hydrogels  
1042  
1043 422 rheological properties as function of the temperature (**Supplementary data Fig. S2**). Indeed,  
1044  
1045 423 interestingly, as the temperature increased from 10 to 60 °C, there was no change of  $G'$  and  $G''$   
1046  
1047 424 of the hydrogel samples. Therefore, physical Cs-based hydrogels, based on the dissolution in  
1048  
1049 425 the alkali/urea aqueous system at low temperatures, exhibited stable rheological properties  
1050  
1051 426 against temperature, regardless the Cs AD or Mw.

1055 427 Such rheological behaviors of Cs-based hydrogels, with interesting elastic and solid  
1056  
1057 428 characteristics, showed the attendance of a promising material for tissue engineering application  
1058  
1059  
1060  
1061

1063  
1064  
1065 429 [55]. Moreover, rapid drug loss prevention and better sustained release properties could be  
1066  
1067 430 potentially provided by high gel strength and short gelation time of the hydrogel, as obtained  
1068  
1069 431 with the Cs-based hydrogels [56].  
1070  
1071

### 1072 **432 3.6.2. Compressive study**

1073  
1074 433 Considering the bone tissue engineering, the mechanical properties of biomaterials like  
1075  
1076 434 hydrogels are design features of priority [57,58]. To have additional insight into the mechanical  
1077  
1078 435 behavior of Cs-based hydrogels, compressive properties were evaluated by exposing wet gels  
1079  
1080 436 to compression testing and the stress vs. strain compressive curves, with different Cs ADs and  
1081  
1082 437 Mws, are shown in **Fig. 4D-F**. Mechanical experimental outcomes display that under  
1083  
1084 438 compression, the compressive strength of the Cs-based hydrogel samples increased with the  
1085  
1086 439 increase in compressive strain for all hydrogel formulations. More particularly, the compressive  
1087  
1088 440 stiffness of Cs-based hydrogels increased concomitantly with the increase of the applied  
1089  
1090 441 compressive strain in the range of 5-7% deformation, and then stuck to rise but in a slower  
1091  
1092 442 manner, indicating that the Cs-based hydrogels were sturdy and ductile.

1093  
1094 443 The order of the mechanical properties was found as: CsIII>CsII>CsI. Indeed, when the  
1095  
1096 444 Cs AD increased from 8% (CsIII based hydrogel) to 17% (CsI based hydrogel), the fracture  
1097  
1098 445 stress values of the Cs-based hydrogels decreased to 0.35 MPa for CsI-0 based hydrogel, while  
1099  
1100 446 values of 0.49 MPa and 0.71 MPa were reached with CsII-0 and CsIII-0 based hydrogels,  
1101  
1102 447 respectively ( $p<0.05$ ). CsIII-3 based hydrogel was found to endure 40% deformation, whereas  
1103  
1104 448 CsII-3 and CsI-3 based hydrogels were capable to bear only 35% and 30% deformation,  
1105  
1106 449 respectively, because of the decrease in the physical crosslink density of the Cs network (**Fig.**  
1107  
1108 450 **4D-F**), suggesting a relatively high strength for CsIII based hydrogel, with the highest  
1109  
1110 451 macromolecular interactions, the most stable network and the smallest pore size [39,59].  
1111  
1112

1113  
1114 452 In another side, the increase in Cs Mw was found to result in a significant enhancement  
1115  
1116 453 in ultimate compressive stress and strain of fracture ( $p<0.05$ ). In fact, hydrogels developed  
1117  
1118  
1119  
1120  
1180

1122  
1123  
1124 454 based on low Mw Cs (CsIII-3, CsII-3 and CsI-3) exhibited mechanical stiffness of more than  
1125  
1126 455 0.29 and 0.27 and 0.11 MPa, respectively. However, ultimate stress modulus increased by 2  
1127  
1128 456 and more than 3-folds for medium (CsIII-2, CsII-2 and CsI-2) and high (CsIII-0, CsII-0 and  
1129  
1130  
1131 457 CsI-0) Mw Cs, respectively (**Fig. 4D-F**). Interestingly, with ADs less than 13% (CsII and CsIII),  
1132  
1133 458 even with medium Mw, based hydrogels kept the structural integrity and stability without  
1134  
1135 459 evidences of any sign of fracture and could recover by themselves subsequently to external  
1136  
1137 460 pressure removal. This finding strongly demonstrated that the synthesized hydrogel exhibited  
1138  
1139 461 interesting mechanical properties, thanks to stiffer chains resulting in stronger pore wall,  
1140  
1141 462 allowing gels thereby to undergo more intense external forces and conditions [33,51,57].  
1142

1143 463 These mechanical data were further consistent with the crystallinity results (**Fig. 3**) and  
1144  
1145 464 the microstructure of the Cs-based hydrogels (**Fig. 1**).  
1146  
1147

### 1148 465 **3.7. Hydrogels *in vitro* degradation behavior**

1149

1150 466 The degradation behavior, based on the weight loss system, was monitored in PBS at pH  
1151  
1152 467 values of 7.4 and 5.5 to simulate the physiological and acidic microenvironments, respectively.  
1153  
1154  
1155 468 Significant differences ( $p < 0.05$ ) were observed, in terms of Cs AD and Mw, considering  
1156  
1157 469 degradation kinetics over 7 days of incubation time (**Fig. 5**). Additionally, the degradation  
1158  
1159 470 behavior patterns were peculiar after immersion under simulated physiological (pH 7.4) and  
1160  
1161 471 acidic (pH 5.5) conditions at 37 °C. However, independently of the swelling conditions and Cs  
1162  
1163 472 characteristics (AD and Mw), more than 75% of the initial mass was preserved (**Fig. 5**).  
1164

1165 473 Independently of Cs characteristics, hydrogels, in PBS of pH 5.5, underwent most quicker  
1166  
1167 474 degradation, compared to samples immersed in PBS of pH 7.4. For example, CsIII-0 based  
1168  
1169 475 hydrogel retained about 91% mass in acidic microenvironment (**Fig. 5A**), and more than 95%  
1170  
1171 476 mass in PBS pH 7.4 (**Fig. 5B**), within 4 days. Qu *et al.* [27], based on the morphology of the  
1172  
1173 477 hydrogels observed under SEM images, proved that differences in degradation behavior could  
1174  
1175 478 be ascribed to an increase in pore sizes, which increased significantly after immersion in PBS.  
1176  
1177  
1178  
1179

1181  
1182  
1183 479 This increase was more pronounced for hydrogels swollen in acidic conditions (PBS of pH 5.5),  
1184  
1185 480 that in the long term, could quick the degradation of hydrogels, due to protonation of chitosan  
1186  
1187 481 amino groups. Indeed, pKa value of D-glucosamine residue is about 6.2~7.0. Subsequently,  
1188  
1189  
1190 482 macromolecular chains bonding become brittle, leading to the hydrogel's networks destruction  
1191  
1192 483 and decomposition.

1193  
1194 484 As expected, Cs-based hydrogels with higher AD and lower Mw exhibited a faster weight  
1195  
1196 485 loss after immersion in both media (PBS of pH 5.5 and pH 7.4). After incubation for 7 days,  
1197  
1198 486 the attained mass losses were about 20%, 22% and 25% for CsI-0, CsI-1 and CsI-3 based  
1199  
1200 487 hydrogels, respectively, while, CsIII based hydrogels still retained more than 80% (CsIII-0),  
1201  
1202 488 78% (CsIII-1) and 75% (CsIII-3) of their original weight, under swelling in pH 5.5 PBS, after  
1203  
1204 489 7 days of incubation time (**Fig. 5A**). These findings corroborate well and directly with the pore  
1205  
1206  
1207 490 diameters distribution based on the SEM images, the swelling and mechanical behaviors of  
1208  
1209 491 prepared hydrogels and the observed crystallinity data. These results proposed that Cs-based  
1210  
1211 492 hydrogels, with good biodegradability and interesting stability in PBS, could exhibit potential  
1212  
1213 493 and promising application in tissue engineering [12,55,59].  
1214

1215 494 During the last decades, smart biomaterials as oral administrative drug carriers attracted  
1216  
1217 495 day-by-day the attention of researchers in the biomedical field [60]. Therefore, Cs-based  
1218  
1219 496 hydrogels developed in the present study could be considered as porous promising pH-sensitive  
1220  
1221 497 biomaterial, with sufficient space for the diffusion of small molecules and drugs, and exercising  
1222  
1223 498 drug release management capability.  
1224  
1225

### 1226 499 **3.8. Optimization of blue crab chitosan concentration for hydrogels construction**

1227

1228 500 An optimization of the ideal concentration of Cs for the formation of hydrogels was  
1229  
1230 501 performed on the basis of the compressive property test and storage modulus determination.  
1231  
1232 502 CsIII-0 based hydrogel was selected for the optimization of Cs concentration study, considering  
1233  
1234 503 its appropriate structural architecture, swelling behavior and mechanical strength.  
1235  
1236  
1237  
1238

1181  
1182  
1183  
1184  
1185  
1186  
1187  
1188  
1189  
1190  
1191  
1192  
1193  
1194  
1195  
1196  
1197  
1198  
1199  
1200  
1201  
1202  
1203  
1204  
1205  
1206  
1207  
1208  
1209  
1210  
1211  
1212  
1213  
1214  
1215  
1216  
1217  
1218  
1219  
1220  
1221  
1222  
1223  
1224  
1225  
1226  
1227  
1228  
1229  
1230  
1231  
1232  
1233  
1234  
1235  
1236  
1237  
1238  
1298

1240  
1241  
1242 504 Mechanical properties of the different Cs-based physical hydrogels, considering the  
1243  
1244 505 compression stress-strain diagrams are illustrated in **Fig. 6A**. The application of a compressive  
1245  
1246 506 force on the hydrogels made it possible to obtain two phases. At low deformation values (around  
1247  
1248 507 5%), an elastic (reversible) deformation was observed as a straight line where the deformation  
1249  
1250 508 was proportional to the stress. Beyond 5%, the stress increased slowly, giving evidence of a  
1251  
1252 509 plastic deformation (irreversible) occurrence, due to the breaking of the bonds or rearrangement  
1253  
1254 510 of the structure [12].  
1255  
1256

1257 511 As displayed in **Fig. 6A**, hydrogel compressive strength was improved with the increase  
1258  
1259 512 of Cs concentration from 0.24 MPa for 1% of Cs to more than 0.48 MPa for hydrogel at 4% of  
1260  
1261 513 Cs. The Cs solution at 1% concentration was found to be not able to form solid physical  
1262  
1263 514 hydrogel and the hydrogel prepared was too weak to be handled and analyzed, mainly due to  
1264  
1265 515 the rather low polymer amount. Indeed, the formed hydrogel was fractured under compressive  
1266  
1267 516 deformation less than 30%. However, hydrogels prepared with more than 2% Cs were already  
1268  
1269 517 relatively rigid and resistant. Further, data revealed that fracture resistance of all hydrogel  
1270  
1271 518 samples was found to be Cs concentration dependent, where 2% Cs-based hydrogel tolerated  
1272  
1273 519 more than 45% of compressive deformation to be fractured, whereas, 50% of compressive  
1274  
1275 520 deformation was not sufficient to induce hydrogels fracture at more than 3% Cs (**Fig. 6A**).  
1276  
1277 521 However, 5% Cs-based hydrogel exhibited a significant decrease in the compressive stress to  
1278  
1279 522 around 0.4 MPa ( $p < 0.05$ ), compared to 3% and 4% Cs-based hydrogels, with an average value  
1280  
1281 523 of 50 MPa.  
1282  
1283

1284 524 In order to further study the influence of Cs concentration on the resulting hydrogels  
1285  
1286 525 structure, their rheological behavior was investigated. The shear ( $G'$ ) and loss ( $G''$ ) moduli  
1287  
1288 526 curves of the Cs-based hydrogels as a function of strain were considered in the rheometer  
1289  
1290 527 dynamic stress environment (**Fig. 6B**).  
1291  
1292  
1293  
1294  
1295  
1296  
1297  
1298  
1299



1299  
1300  
1301 528 Profiles displayed that  $G'$  values of Cs-based hydrogels increased with the increase of Cs  
1302  
1303 529 concentration, with an increasing strain from 0.1% to 1000%. In fact,  $G'$  of Cs 1%-based  
1304  
1305 530 hydrogel ( $15.9 \cdot 10^3$  Pa) at 100% strain was 11.3 times lower than that of Cs 4%-based hydrogel  
1306  
1307 (181  $\cdot 10^3$  Pa). Although, in all cases, the storage modulus  $G'$  was below the loss modulus  $G''$ ,  
1308 531 indicating a predominantly gel-like behavior, the storage modulus  $G'$  decreased significantly  
1309  
1310 532 ( $p < 0.05$ ), reaching  $63.2 \cdot 10^3$  Pa, for higher concentration of Cs (5%). In another aspect, 1% Cs-  
1311  
1312 533 based hydrogel was found to be able to support only around 123% deformation and maintain  
1313  
1314 534 the gel-like behavior (the point at which  $G'' > G'$ ), while 3% and 4% Cs-based hydrogels were  
1315  
1316 535 capable to bear more than 574% and 491% deformation, respectively. However, at higher Cs  
1317  
1318 536 content, the gel structure was kept only at strains below 185% (**Fig. 6B**).

1322  
1323 538 Consequently, from the mechanical and rheological testing data, 3% Cs-based hydrogel  
1324  
1325 539 exhibited better rheological properties than those of 2% Cs, and the fracture deformation was  
1326  
1327 540 greater than that of 5% Cs. Similarly, excessive Cs concentration led to thicker and too rigid  
1328  
1329 541 hydrogel, which could be attributed to chains entanglements excess, leading to hydrogels  
1330  
1331 542 brittleness [61]. However, due to the gradually improved number of the hydrogen-bonded  
1332  
1333 543 crosslink regions between the Cs chains, in a relatively concentrated solution, aggregation and  
1334  
1335 544 entanglement amongst the Cs macromolecular chains will significantly took place.

1337 545 Therefore, 3% concentration of chitosan solution was carefully chosen to elaborate Cs-  
1338  
1339 546 based hydrogels in the following section, for the Riboflavin *in vitro* release study.

### 1342 547 **3.9. Encapsulation of riboflavin, *in vitro* loading and release profiles**

1343  
1344 548 Hydrogels structure is characterized by three major parameters, namely the volume  
1345  
1346 549 fraction of polymer in the inflated state, the average molecular weight of based polymers as  
1347  
1348 550 well as the pore size distribution of the network [9-10]. This architecture of hydrogels allows  
1349  
1350 551 the diffusion of molecules of different sizes in the network, which makes these biomaterials  
1351  
1352 552 interesting for drug release applications [7,12].

1358  
1359  
1360 553 As the model drug, the kinetics of riboflavin release, through the Cs-based hydrogels were  
1361  
1362 554 monitored based on the cumulative amounts of released riboflavin as a function of time.  
1363  
1364 555 Different concentrations of riboflavin (1-5 g/l) were used to investigate the influence of drug  
1365  
1366 concentration on EE and release profiles.  
1367 556  
1368  
1369 557 The EE and LC of Cs-hydrogels for riboflavin, as reported in **Table 3**, were found to be  
1370  
1371 558 drug concentration-dependent ( $p < 0.05$ ). Indeed, the EE values increased from more than 75%  
1372  
1373 559 for 1 g/l of riboflavin to about 85% for 3 g/l of riboflavin. However, above 3 g/l of riboflavin,  
1374  
1375 560 the EE dropped dramatically to 68% and 56%, for 4 g/l and 5 g/l of riboflavin, respectively.  
1376  
1377 561 Regarding the LC of riboflavin, values increased concomitantly with the increase of drug  
1378  
1379 562 concentration from 24% for 1 g/l of riboflavin to the saturated capacity of 37% at 3 g/l of  
1380  
1381 563 riboflavin ( $p < 0.05$ ). No significant differences in the riboflavin LC values was noted beyond 3  
1382  
1383 g/l of riboflavin ( $p \geq 0.05$ ). The decrease in the amount of encapsulated riboflavin at high  
1384 564  
1385 concentration could be related to the saturation of hydrogel (limitation of riboflavin loading  
1386 565  
1387 into Cs-based hydrogel), since the encapsulation of riboflavin was monitored through its  
1388 566  
1389 diffusion in the hydrogel network.  
1390 567  
1391

1392 568 Riboflavin release profiles from Cs-based hydrogels, at 37 °C, in HCl-NaOH (0.1 M), pH  
1393  
1394 569 5.5, exhibited deliverance patterns, characterized by an initial short-time rapid release, during  
1395  
1396 570 the first 8 h, followed by low riboflavin release to 72 h. Beyond 72 h, the rate of released  
1397  
1398 riboflavin tended to stabilize (**Fig. 7**). Data reveal that hydrogel with lower riboflavin charge  
1399 571  
1400 showed high initial release in terms of percentage. Indeed, at a riboflavin concentration of 1 g/l,  
1401 572  
1402 the initial release rate (after 4 h) was 11% relative to the amount of initial riboflavin loaded in  
1403 573  
1404 the hydrogel. It was of 46% and 79%, after 24 h and at the end of the study (96 h). Regarding  
1405 574  
1406 a concentration of 5 g/l, the release of riboflavin was 5%, 18% and 36%, after 4 h, 24 h and 96  
1407 575  
1408 h, respectively. In terms of the total mass of riboflavin released, the hydrogel group with higher  
1409 576  
1410 charge released more riboflavin. For example, at a riboflavin concentration of 1 g/l, the amount  
1411 577  
1412  
1413  
1414  
1415

1417  
1418  
1419 578 released riboflavin was 790 mg after 96 h, while for the 5 g/l riboflavin hydrogel group, about  
1420  
1421 579 2 g of riboflavin were released (**Fig. 7A**). This finding could be assigned to the concentration  
1422  
1423  
1424 580 gradient phenomenon as diffusion management force. The more Riboflavin loading increased,  
1425  
1426 581 the higher concentration gradient increased [27].  
1427

1428 582 The riboflavin (3 g/l) release patterns were further investigated in HCl-NaCl (0.1 M)  
1429  
1430 583 under different pH conditions (pH 2.0, pH 4.5 and pH 7.4). Deliverance curves, as reported in  
1431  
1432 584 **Fig. 7B**, showed that riboflavin was barely released from the Cs-based hydrogels, at pH 7.4, of  
1433  
1434 585 only 13% after 4 days of incubation. However, high amounts of riboflavin were released in  
1435  
1436 586 acidic pH ( $p < 0.05$ ), further, the amount of released riboflavin from Cs-based hydrogels was  
1437  
1438 587 higher in pH than pH 4.5 in pH 2.0. Indeed, 16% and 38% of riboflavin were released from Cs-  
1439  
1440  
1441 588 based hydrogel, after 8 h, at pH 4.5 and pH 2.0, respectively. Therefore, Cs-hydrogels were  
1442  
1443 589 found to release significantly more riboflavin in acidic microenvironments, probably due to  
1444  
1445 590 higher swelling rates or exhaustive hydrogels structure destruction and thereby faster  
1446  
1447 591 degradation and release of riboflavin [26,59,60].  
1448  
1449

#### 1450 592 4. Conclusion

1451  
1452 593 Different Cs-based hydrogels were successfully engineered, considering Cs AD and Mw,  
1453  
1454 594 based on the alkali/urea aqueous system following the freezing/thawing/solvent evaporation  
1455  
1456 595 approach. As expected, hydrogels pore size distribution, mechanical strength, swelling and  
1457  
1458 596 thermal resistance behaviors besides the *in vitro* biodegradation patterns, were extremely  
1459  
1460 597 depending on Cs structural characteristics. Low AD coupled with high Mw seemed to be very  
1461  
1462 598 interesting for the development of promoting biomaterials with stable and appropriate features.  
1463

1464 599 Moreover, Cs-based hydrogels were monitored to study the *in vitro* release of riboflavin  
1465  
1466 600 selected as the model drug. The obtained release patterns displayed that Cs-based hydrogels  
1467  
1468  
1469 601 could be applied as smart pH-sensitive carrier for drug-controlled release for further biomedical  
1470  
1471 602 applications (antitumor, protein and peptide, gene and antibiotic drug delivery). Additionally,  
1472  
1473  
1474

1476  
1477  
1478  
1479  
1480  
1481  
1482  
1483  
1484  
1485  
1486  
1487  
1488  
1489  
1490  
1491  
1492  
1493  
1494  
1495  
1496  
1497  
1498  
1499  
1500  
1501  
1502  
1503  
1504  
1505  
1506  
1507  
1508  
1509  
1510  
1511  
1512  
1513  
1514  
1515  
1516  
1517  
1518  
1519  
1520  
1521  
1522  
1523  
1524  
1525  
1526  
1527  
1528  
1529  
1530  
1531  
1532  
1533  
1475

603 due to its suitable structural architecture, swelling behavior and mechanical strength, the  
604 application of Cs-based hydrogels seems to be a very interesting alternative in the tissue  
605 engineering field.

### 606 Acknowledgement

607 The present work was funded by the Ministry of Higher Education and Scientific  
608 Research, Tunisia.

### 609 References

- 610 1. B. Tavsanlı, O. Okay. Mechanically Robust and Stretchable Silk/hyaluronic Acid  
611 Hydrogels. *Carbohydr. Polym* 2019, 208, 413-420.
- 612 2. M. Khan, J.T. Koivisto, T.I. Hukka, M. Hokka, M. Kellomäki. Composite Hydrogels Using  
613 Bioinspired Approach With In Situ Fast Gelation and Self-healing Ability as Future  
614 Injectable Biomaterial. *ACS Appl. Mater. Interfaces* 2018, 10, 11950-11960.
- 615 3. N. Martin, G. Youssef. Dynamic Properties of Hydrogels and Fiber-reinforced Hydrogels.  
616 *J. Mech. Behav. Biomed. Mater* 2018, 85, 194-200.
- 617 4. S. Ma, B. Yu, X. Pei, F. Zhou. Structural Hydrogels. *Polymer* 2016, 98, 516-535.
- 618 5. J. Duan, X. Liang, Y. Cao, Se. Wang, Zhang, L. High Strength Chitosan Hydrogels with  
619 Biocompatibility via New Avenue Based on Constructing Nanofibrous Architecture.  
620 *Macromolecules* 2015, 48, 2706-2714.
- 621 6. W. Wang, Y. Zhao, H. Yi, T. Chen, S. Kang, T. Zhang, F. Rao, S. Song. Pb(II) Removal  
622 from Water Using Porous Hydrogel of Chitosan-2D Montmorillonite. *Int. J. Biol. Macromol*  
623 2019, 128, 85-93.
- 624 7. L. Liu, Q. Gao, X. Lu, H. Zhou. In Situ Forming Hydrogels Based on Chitosan for Drug  
625 Delivery and Tissue Regeneration. *Asian J. Pharm. Sci* 2016, 11, 673-683.
- 626 8. Y.H. Cheng, Y.C. Ko, Y.F. Chang, S.H. Huang, C.J.L. Liu. Thermosensitive Chitosan-  
627 gelatin-based Hydrogel Containing Curcumin-loaded Nanoparticles and Latanoprost as a  
628 Dual-drug Delivery System for Glaucoma Treatment. *Exp. Eye Res* 2019, 179, 179-187.
- 629 9. R. Dimatteo, N.J. Darling, T. Segura. In Situ Forming Injectable Hydrogels for Drug  
630 Delivery and Wound Repair. *Adv. Drug Deliv. Rev* 2018, 127, 167-184.
- 631 10. T.M. Aminabhavi, S.P. Dharupaneedi. Production of Chitosan-based Hydrogels for  
632 Biomedical Applications. *Chitosan Based Biomaterials Volume 1 – Fundamentals* 2017,  
633 295-319.
- 634 11. A.M. Slavutsky, M.A. Bertuzzi, Formulation and Characterization of Hydrogel Based on  
635 Pectin and Brea Gum. *Int. J. Biol. Macromol* 2019, 123, 784-791.
- 636 12. Z. Huang, C. Gao, Y. Huang, X. Zhang, X. Deng, Q. Cai. Injectable  
637 polyphosphazene/gelatin hybrid hydrogel for biomedical applications. *Mater. Des* 2008,  
638 160, 1137-1147.



1535  
1536  
1537  
1538  
1539  
1540  
1541  
1542  
1543  
1544  
1545  
1546  
1547  
1548  
1549  
1550  
1551  
1552  
1553  
1554  
1555  
1556  
1557  
1558  
1559  
1560  
1561  
1562  
1563  
1564  
1565  
1566  
1567  
1568  
1569  
1570  
1571  
1572  
1573  
1574  
1575  
1576  
1577  
1578  
1579  
1580  
1581  
1582  
1583  
1584  
1585  
1586  
1587  
1588  
1589  
1590  
1591  
1592  
1593

- 639 13. Annu, K. Manzoor, S. Ahmad, A. Soundarajan, S. Ikram, S. Ahmed. Chitosan Based  
640 Nanomaterials for Biomedical Applications. *Handbook of Nanomaterials for Industrial*  
641 *Applications, Micro and Nano Technologies* 2018, 543-562.
- 642 14. B. Choi, S. Kim, B. Lin, B.M. Wu, M. Lee. Cartilaginous Extracellular Matrix-Modified  
643 Chitosan Hydrogels for Cartilage Tissue Engineering. *ACS Appl. Mater. Interfaces* 2014, 6,  
644 20110–20121.
- 645 15. E. Calo, V.V. Khutoryanskiy. Biomedical Applications of Hydrogels: A Review of Patents  
646 and Commercial Products. *Eur. Polym. J* 2015, 65, 252-267.
- 647 16. G. Camci-Unal, P. Zorlutuna, A. Khademhosseini. Chapter 4 - Fabrication of Microscale  
648 Hydrogels for Tissue Engineering Applications. *Biofabrication, Micro- and Nano-*  
649 *fabrication, Printing, Patterning and Assemblies* 2013, 59-80.
- 650 17. S.Z. Md Rasib, H. Md Akil, A. Khan, Z.A.A. Hamid. Controlled Release Studies Through  
651 Chitosan-based Hydrogel Synthesized at Different Polymerization Stages. *Int. J. Biol.*  
652 *Macromol* 2019, 128, 531-536.
- 653 18. F.A. Fookes, L.N. Mengatto, A. Rigalli, J.A. Luna. Controlled Fluoride Release for  
654 Osteoporosis Treatment Using Orally Administered Chitosan Hydrogels. *J. Drug Deliv. Sci.*  
655 *Technol* 2019, 51, 268-275.
- 656 19. B. Onat, S. Ulasan, S. Banerjee, E. Erel-Goktepe. Multifunctional Layer-by-layer Modified  
657 Chitosan/poly(Ethylene Glycol) Hydrogels. *Eur. Polym. J* 2019, 112, 73-86.
- 658 20. K. Saekhor, W. Udomsinprasert, S. Honsawek, W. Tachaboonyakiat. Preparation of an  
659 Injectable Modified Chitosan-based Hydrogel Approaching for Bone Tissue Engineering.  
660 *Int. J. Biol. Macromol* 2019, 123, 167-173.
- 661 21. M. Hamdi, S. Hajji, S. Affes, W. Taktak, H. Maâlej, M. Nasri, R. Nasri. Development of a  
662 Controlled Bioconversion Process for The Recovery of Chitosan from Blue Crab (*Portunus*  
663 *segnis*) Exoskeleton. *Food Hydrocoll* 2018, 77, 534-548.
- 664 22. S.H. Chang, H.T.V. Lin, G.J. Wu, G.J. Tsai. pH Effects on Solubility, Zeta Potential, And  
665 Correlation Between Antibacterial Activity and Molecular Weight of Chitosan. *Carbohydr.*  
666 *Polym* 2015, 134, 74-81.
- 667 23. R.Q. Qian, R.W. Glanville. Methods for Purifying Chitosan. *US Patent* 2005, 6896809.
- 668 24. B. Huang, M. Liu, C. Zhou. Chitosan Composite Hydrogels Reinforced with Natural Clay  
669 Nanotubes. *Carbohydr. Polym* 2017, 175, 689-698.
- 670 25. AOAC. Official Methods of Analysis (17th ed.). Washington, DC: *Association of Official*  
671 *Analytical Chemists* 2000.
- 672 26. S. Yu, X. Zhang, G. Tan, L. Tian, D. Liu, Y. Liu, X. Yang, W. Pan. A Novel pH-Induced  
673 Thermosensitive Hydrogel Composed of Carboxymethyl Chitosan and Poloxamer Cross-  
674 Linked by Glutaraldehyde for Ophthalmic Drug Delivery. *Carbohydr. Polym* 2017, 155,  
675 208–217.
- 676 27. J. Qu, X. Zhao, P.X. Ma, B. Guo. pH-Responsive Self-Healing Injectable Hydrogel Based  
677 On N-Carboxyethyl Chitosan for Hepatocellular Carcinoma Therapy. *Acta Biomater* 2017,  
678 58, 168-180.
- 679 28. B. Wang, B. Adhikari, C.J. Barrow. Highly Stable Spray Dried Tuna Oil Powders  
680 Encapsulated in Double Shells of Whey Protein Isolate-Agar Gum and Gellan Gum  
681 Complex Coacervates. *Powder Technol* 2018, In Press, Corrected Proof.

1594  
1595  
1596  
1597  
1598  
1599  
1600  
1601  
1602  
1603  
1604  
1605  
1606  
1607  
1608  
1609  
1610  
1611  
1612  
1613  
1614  
1615  
1616  
1617  
1618  
1619  
1620  
1621  
1622  
1623  
1624  
1625  
1626  
1627  
1628  
1629  
1630  
1631  
1632  
1633  
1634  
1635  
1636  
1637  
1638  
1639  
1640  
1641  
1642  
1643  
1644  
1645  
1646  
1647  
1648  
1649  
1650  
1651  
1652

29. H. Ge, T. Hua, J. Wang. Preparation and Characterization of Poly (Itaconic Acid)-Grafted Crosslinked Chitosan Nanoadsorbent For High Uptake of Hg<sup>2+</sup> And Pb<sup>2+</sup>. *Int. J. Biol. Macromol* 2017, 95, 954-961.
30. A.M. Heimbuck, T.R. Priddy-Arrington, B.J. Sawyer, M.E. Caldorera-Moore. Effects of Post-Processing Methods on Chitosan-Genipin Hydrogel Properties. *Mater. Sci. Eng. C* 2019, 98, 612–618.
31. M.C.G. Pella, M.K. Lima-Tenorio, E.T. Tenorio-Neto, M.R. Guilherme, E.C. Muniz, A.F. Rubira. Chitosan-Based Hydrogels: From Preparation to Biomedical Applications. *Carbohydr. Polym* 2018, 196, 233-245.
32. M.L. Tsai, H.W. Chang, H.C. Yu, Y.S. Lin, Y.D. Tsai. Effect of Chitosan Characteristics and Solution Conditions on Gelation Temperatures of Chitosan/2-Glycerophosphate/Nanosilver Hydrogels. *Carbohydr. Polym* 2011, 84, 1337-1343.
33. F. Wang, Y. Wen, T. Bai. The Composite Hydrogels of Polyvinyl Alcohol–Gellan Gum Ca<sup>2+</sup> With Improved Network Structure and Mechanical Property. *Mater. Sci. Eng. C* 2016, 69, 268–275.
34. B. Ding, H. Gao, J. Song, Y. Li, L. Zhang, X. Cao, M. Xu, J. Cai. Tough and Cell-Compatible Chitosan Physical Hydrogels for Mouse Bone Mesenchymal Stem Cells *in Vitro*. *ACS Appl. Mater. Interfaces* 2016, 10, 19739-19746.
35. Y. Yao, M. Xia, H. Wang, G. Li, H. Shen, G. Ji, Q. Meng, Y. Xie. Preparation and Evaluation of Chitosan-Based Nanogels/Gels for Oral Delivery of Myricetin. *Eur. J. Pharm. Sci* 2016, 91, 144-153.
36. L. Zhang, Y. Li, L. Li, B. Guo, P.X. Ma. Non-Cytotoxic Conductive Carboxymethyl-Chitosan/Aniline Pentamer Hydrogels. *React. Funct. Polym* 2014, 82, 81-88.
37. X. Zhao, P. Li, B. Guo, P.X. Ma. Antibacterial and Conductive Injectable Hydrogels Based on Quaternized Chitosan-Graft-Polyaniline/Oxidized Dextran for Tissue Engineering. *Acta Biomater* 2015, 26, 236-248.
38. C. Chang, S. Chen, L. Zhang. Novel Hydrogels Prepared Via Direct Dissolution of Chitin at Low Temperature: Structure and Biocompatibility. *J. Mater. Chem* 2011, 21, 3865-3872.
39. E. Assaad, M. Maire, S. Lerouge. Injectable Thermosensitive Chitosan Hydrogels with Controlled Gelation Kinetics and Enhanced Mechanical Resistance. *Carbohydr. Polym* 2015, 130, 87–96.
40. Q. Wang, S. Chen, D. Chen. Preparation and Characterization of Chitosan Based Injectable Hydrogels Enhanced by Chitin Nano-Whiskers. *J. Mech. Behav. Biomed. Mater* 2017, 65, 466–477.
41. M. Fan, Q. Hu. Superadsorption Of LiOH Solution on Chitosan as A New Type of Solvent for Chitosan by Freezing/Blasting. *Carbohydr. Polym* 2013, 94, 430– 435.
42. L. Cui, J. Jia, Y. Guo, Y. Liu, P. Zhu. Preparation and Characterization of IPN Hydrogels Composed of Chitosan and Gelatin Cross-Linked by Genipin. *Carbohydr. Polym* 2014, 99, 31-38.
43. X.J. Liu, Y. Chen, Q.L. Huang, W. He, Q.L. Feng, B. Yu. A Novel Thermo-Sensitive Hydrogel Based on Thiolated Chitosan/Hydroxyapatite/Beta-Glycerophosphate. *Carbohydr. Polym* 2014, 110, 62-9.
44. Y. Ogawa, S. Kimura, M. Wada, S. Kuga. Crystal analysis and high-resolution imaging of microfibrillar  $\alpha$ -chitin from *Phaeocystis*. *J. Struct. Biol* 2010, 171, 111–116.

1653  
1654  
1655  
1656  
1657  
1658  
1659  
1660  
1661  
1662  
1663  
1664  
1665  
1666  
1667  
1668  
1669  
1670  
1671  
1672  
1673  
1674  
1675  
1676  
1677  
1678  
1679  
1680  
1681  
1682  
1683  
1684  
1685  
1686  
1687  
1688  
1689  
1690  
1691  
1692  
1693  
1694  
1695  
1696  
1697  
1698  
1699  
1700  
1701  
1702  
1703  
1704  
1705  
1706  
1707  
1708  
1709  
1710  
1793

- 726 45. N. Vasanthan, I.D. Shin, A.E. Tonelli. Structure, Conformation, And Motions Of  
727 Poly(Ethylene Oxide) And Poly(Ethylene Glycol) In Their Urea Inclusion Compounds.  
728 *Macromolecules* 1996, 29, 263–267.
- 729 46. A.L. Skwarczynska, D. Binias, W. Maniukiewicz, Z. Modrzejewska, T.E.L. Douglas. The  
730 Mineralization Effect on Chitosan Hydrogel Structure Containing Collagen and Alkaline  
731 Phosphatase. *J. Mol. Struct* 2019, 1187, 86-97.
- 732 47. Y. Liu, Z. Liu, W. Pan, Q. Wu. Absorption Behaviors and Structure Changes of Chitin in  
733 Alkali Solution. *Carbohydr. Polym* 2008, 72, 235–239.
- 734 48. X. Liang, J. Duan, Q. Xu, X. Wei, A. Lu, L. Zhang. Ampholytic Microspheres Constructed  
735 from Chitosan and Carrageenan in Alkali/Urea Aqueous Solution for Purification of Various  
736 Wastewater. *Chem. Eng. J* 2017, 317, 766-776.
- 737 49. H.Y. Zhou, L.J. Jiang, P.P. Cao, J.B. Li, X.G. Chen. Glycerophosphate-Based Chitosan  
738 Thermosensitive Hydrogels and Their Biomedical Applications. *Carbohydr. Polym* 2015,  
739 117, 524-53.
- 740 50. M.R. Saboktakin, R.M. Tabatabaie, A. Maharramov, M.L. Ramazanov. Synthesis And In  
741 Vitro Studies of Biodegradable Thiolated Chitosan Hydrogels for Breast Cancer Therapy.  
742 *Int. J. Biol. Macromol* 2011, 48, 747-752.
- 743 51. Y. Xie, X. Liao, J. Zhang, F. Yang, Z. Fan. Novel Chitosan Hydrogels Reinforced by Silver  
744 Nanoparticles with Ultrahigh Mechanical and High Antibacterial Properties for Accelerating  
745 Wound Healing. *Int. J. Biol. Macromol* 2018, 119, 402-412.
- 746 52. M.A. Gamiz-González, D.M. Correia, S. Lanceros-Mendez, V. Sencadas, J.L. Gómez  
747 Ribelles, A. Vidaurre. Kinetic Study of Thermal Degradation of Chitosan as A Function of  
748 Deacetylation Degree. *Carbohydr. Polym* 2017, 167, 52-58.
- 749 53. Z. Bao, C. Jiang, Z. Wang, Q. Ji, G. Sun, S. Bi, Y. Liu, X. Chen. The Influence of Solvent  
750 Formulations on Thermosensitive Hydroxybutyl Chitosan Hydrogel as A Potential Delivery  
751 Matrix for Cell Therapy. *Carbohydr. Polym* 2017, 170, 80-88.
- 752 54. J. Maity, S.K. Ray. Removal of Cu (II) Ion from Water Using Sugar Cane Bagasse  
753 Cellulose and Gelatin Based Composite Hydrogels. *Int. J. Biol. Macromol* 2016, 97, 238-  
754 248.
- 755 55. S. Bi, Z. Bao, X. Bai, S. Hu, X. Cheng, X. Chen. Tough Chitosan Hydrogel Based on  
756 Purified Regeneration and Alkaline Solvent as Biomaterials for Tissue Engineering  
757 Applications. *Int. J. Biol. Macromol* 2017, 104, 224-231.
- 758 56. F. Wahid, X.H. Hu, L.Q. Chu, S.R. Jia, Y.Y. Xie, C. Zhong. Development of Bacterial  
759 Cellulose/Chitosan Based Semi-Interpenetrating Hydrogels with Improved Mechanical and  
760 Antibacterial Properties. *Int. J. Biol. Macromol* 2019, 122, 380-387.
- 761 57. Z. Naghizadeh, A. Karkhaneh, A. Khojasteh. Self-Crosslinking Effect of Chitosan and  
762 Gelatin on Alginate-Based Hydrogels: Injectable in Situ Forming Scaffolds. *Mater. Sci. Eng.*  
763 *C* 2018, 89, 256-264.
- 764 58. C. Chang, M. He, J. Zhou, L. Zhang. Swelling Behaviors of pH- and Salt-Responsive  
765 Cellulose-Based Hydrogels. *Macromolecules* 2011, 44, 1642–1648.
- 766 59. S. Zang, R. Mu, F. Chen, X. Wei, L. Zhu, B. Han, H. Yu, B. Bi, B. Chen, Q. Wang, L. Jin.  
767 Injectable Chitosan/B-Glycerophosphate Hydrogels with Sustained Release Of BMP-7 And  
768 Ornidazole In Periodontal Wound Healing of Class III Furcation Defects. *Mater. Sci. Eng.*  
769 *C* 2019, 99, 919-928.



1712  
1713  
1714  
1715  
1716  
1717  
1718  
1719  
1720  
1721  
1722  
1723  
1724  
1725  
1726  
1727  
1728  
1729  
1730  
1731  
1732  
1733  
1734  
1735  
1736  
1737  
1738  
1739  
1740  
1741  
1742  
1743  
1744  
1745  
1746  
1747  
1748  
1749  
1750  
1751  
1752  
1753  
1754  
1755  
1756  
1757  
1758  
1759  
1760  
1761  
1762  
1763  
1764  
1765  
1766  
1767  
1768  
1769  
1770

770 60. Y. Ren, X. Zhao, X. Liang, P.X. Ma, B. Guo. Injectable Hydrogel Based on Quaternized  
771 Chitosan, Gelatin and Dopamine as Localized Drug Delivery System to Treat Parkinson's  
772 Disease. *Int. J. Biol. Macromol* 2017, 105, 1079-1087.  
773 61. D. Zhao, J. Huang, Y. Zhong, K. Li, L. Zhang, J. Cai. High-Strength and High-Toughness  
774 Double-Cross-Linked Cellulose Hydrogels: A New Strategy Using Sequential Chemical and  
775 Physical Cross-Linking. *Adv. Funct. Mater* 2016, 26, 1-9.

## **Figure captions**

**Figure 1:** SEM images of Cs-based hydrogels (GCs) cross sections: GCsI-0 with AD of 17% and Mw of 125.6 kDa (**A**), GCsI-1 with AD of 17% and Mw of 17.8 kDa, (**B**) GCsI-3 with AD of 17% and Mw of 10.44 kDa (**C**), GCsII-0 with AD of 13% and Mw of 118.9 kDa (**D**), GCsII-1 with AD of 13% and Mw of 59.27 kDa (**E**), GCsII-3 with AD of 13% and Mw of 18.54 kDa (**F**), GCsIII-0 with AD of 8% and Mw of 115 kDa (**G**), GCsIII-1 with AD of 8% and Mw of 78.43 kDa (**H**) and GCsIII-3 with AD of 8% and Mw of 16.04 kDa (**I**).

**Figure 2:** ATR-FTIR profiles of Cs-based hydrogels (GCs) with different AD and Mw, (**A**) GCsI, (**B**) GCsII and (**C**) GCsIII, compared to Cs powders spectra.

**Figure 3:** XRD patterns of Cs-based hydrogels (GCs) with different AD and Mw, (**A**) GCsI, (**B**) GCsII and (**C**) GCsIII, compared to Cs powders spectra.

**Figure 4:** Mechanical features of Cs-based hydrogels (GCs) as function of Cs AD and Mw. Rheological behavior (**A**) GCsI, (**B**) GCsII, (**C**) GCsIII,  $f=1$  Hz,  $T=37$  °C. Compressive properties, at a temperature of 25 °C and a compression speed of 1 mm/min, (**D**) GCsI, (**E**) GCsII, (**F**) GCsIII.

**Figure 5:** *In vitro* biodegradation Cs-based hydrogels (GCs) as function of Cs AD and Mw, in PBS at (**A**) pH 5.5 (acidic microenvironment) and (**B**) pH 7.4 (physiological microenvironment simulation), at 37 °C.

**Figure 6:** Mechanical behavior of Cs-based hydrogels as function of Cs concentration. (**A**) Compressive stress vs. compressive strain profiles. (**B**) Viscoelastic properties patterns as function of strain (%),  $f=1$  Hz,  $T=37$  °C.

**Figure 7:** Riboflavin, as the model drug, *in vitro* release profile and kinetics from Cs-based hydrogels. Riboflavin incorporation was monitored by immersion in riboflavin solution (0-5 g/l) in dark at 5 °C for 48 h. The release tests were performed in HCl and NaCl (0.1 M) with different pH values (pH 2.0, pH 4.5 and pH 7.4) at 37 °C. (**A**) Riboflavin release kinetics at different concentrations (0-5 g/l of riboflavin) in pH 5.5. (**B**) Riboflavin (3 g/l) release kinetics at different pH values (pH 2.0, pH 4.5 and pH 7.4).

**Fig. 1**

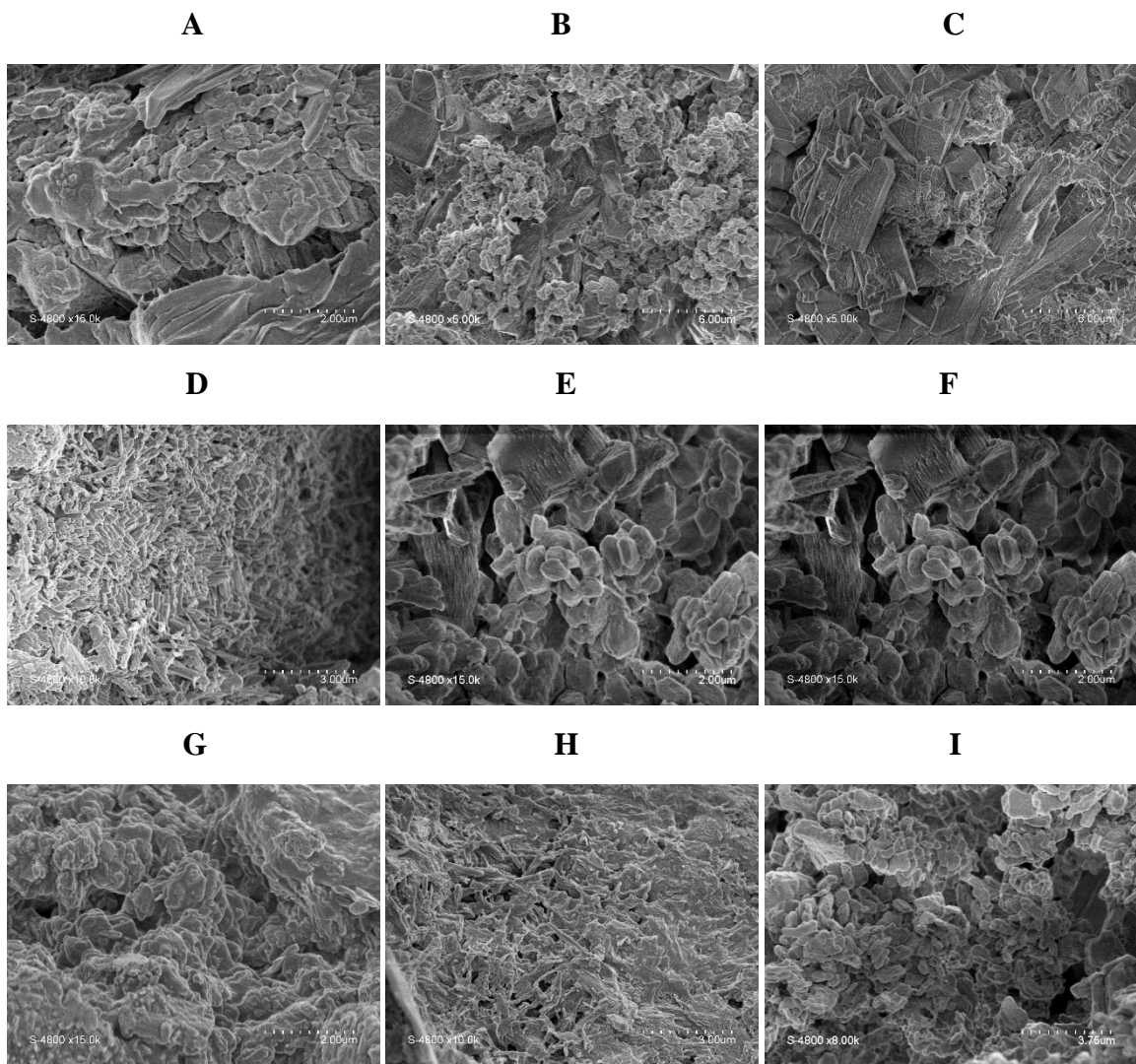


**Fig. 2**

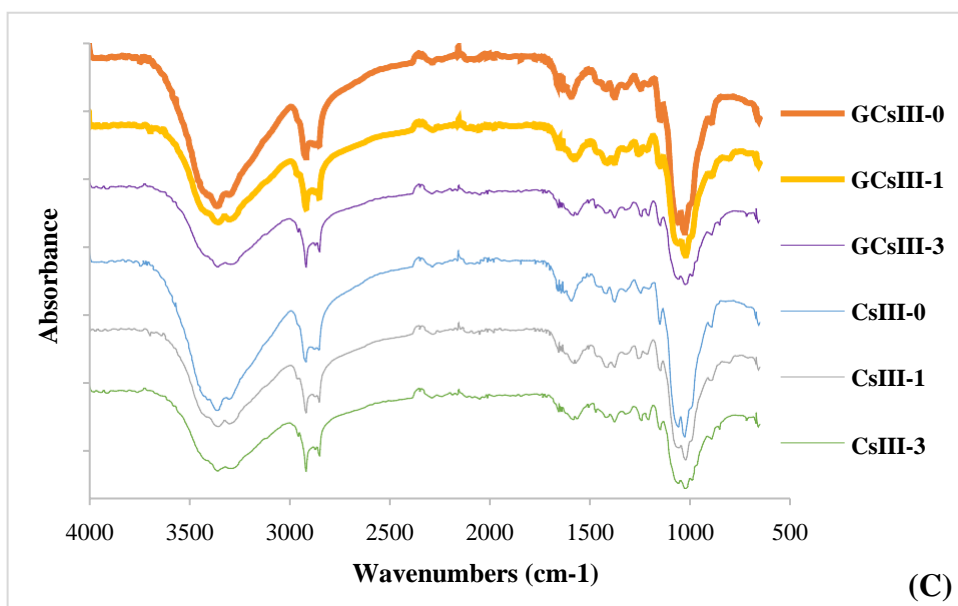
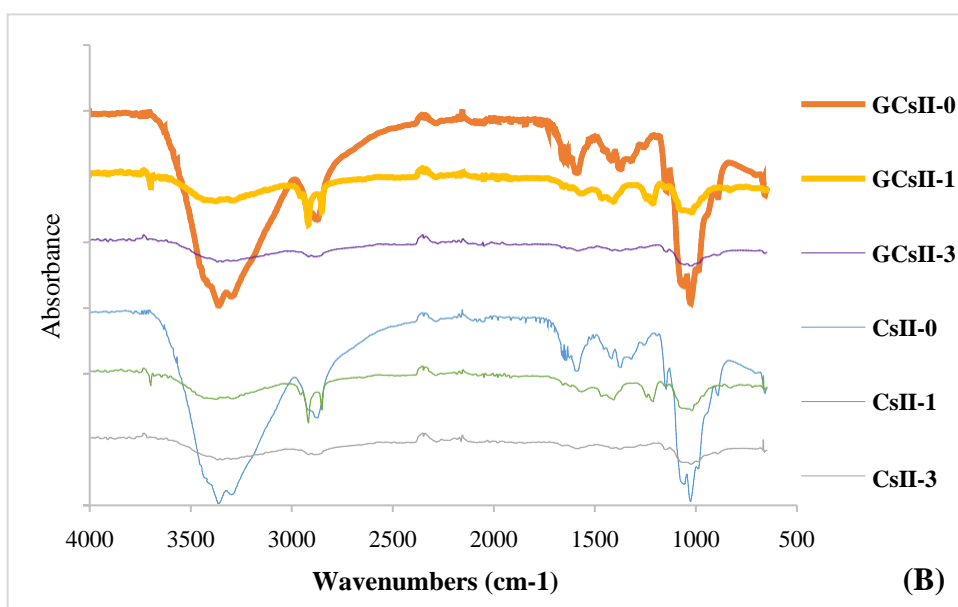
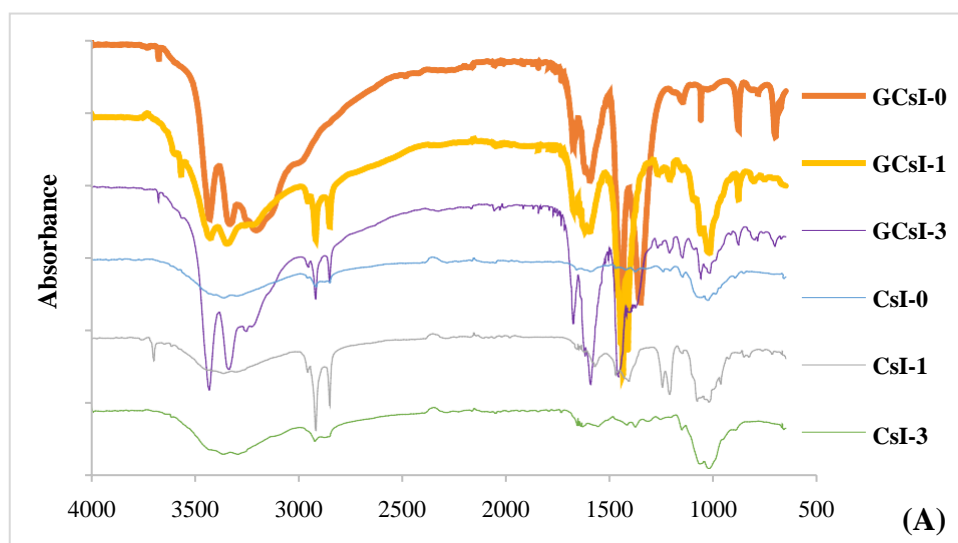
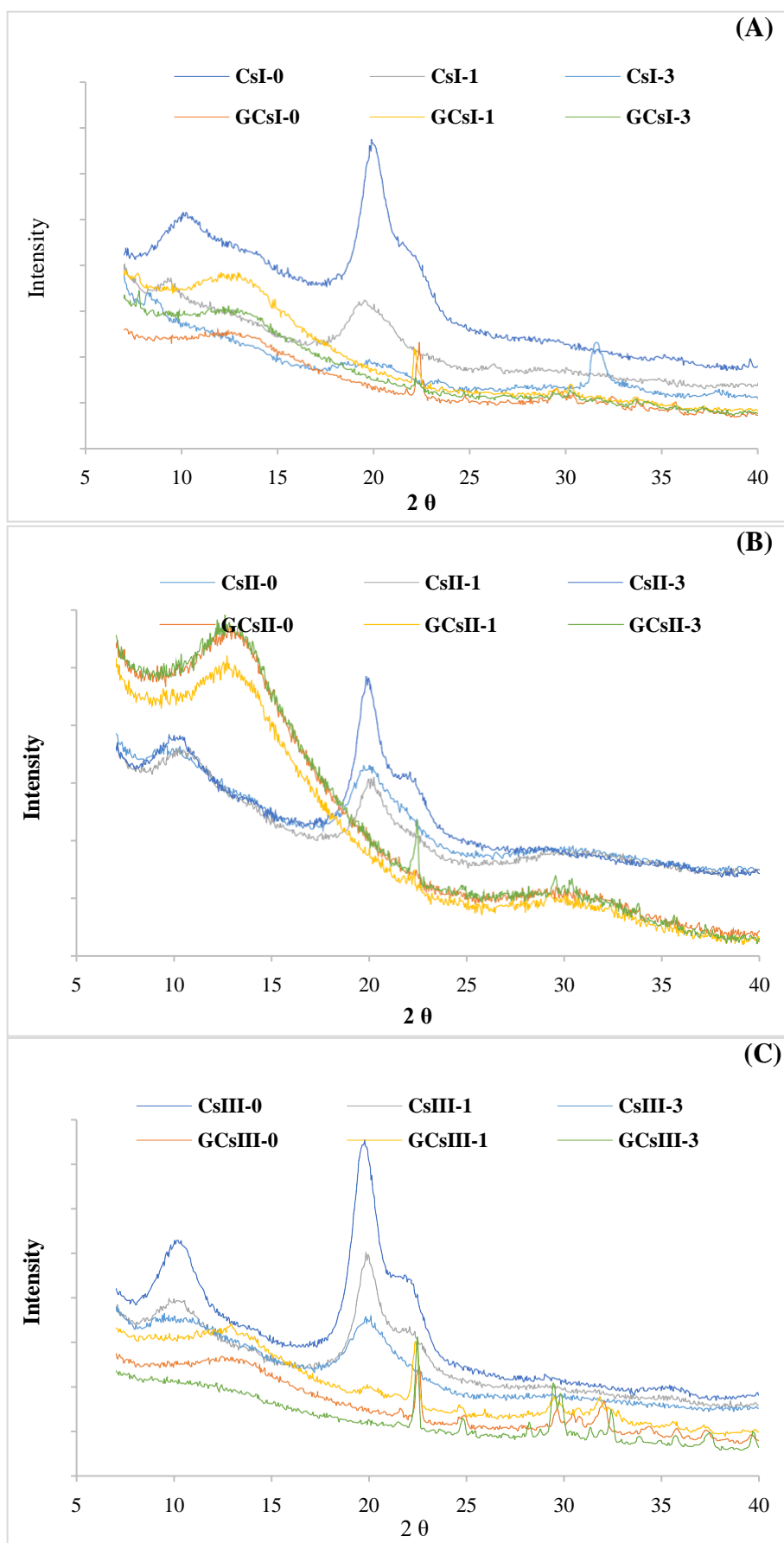


Fig. 3



**Fig. 4**

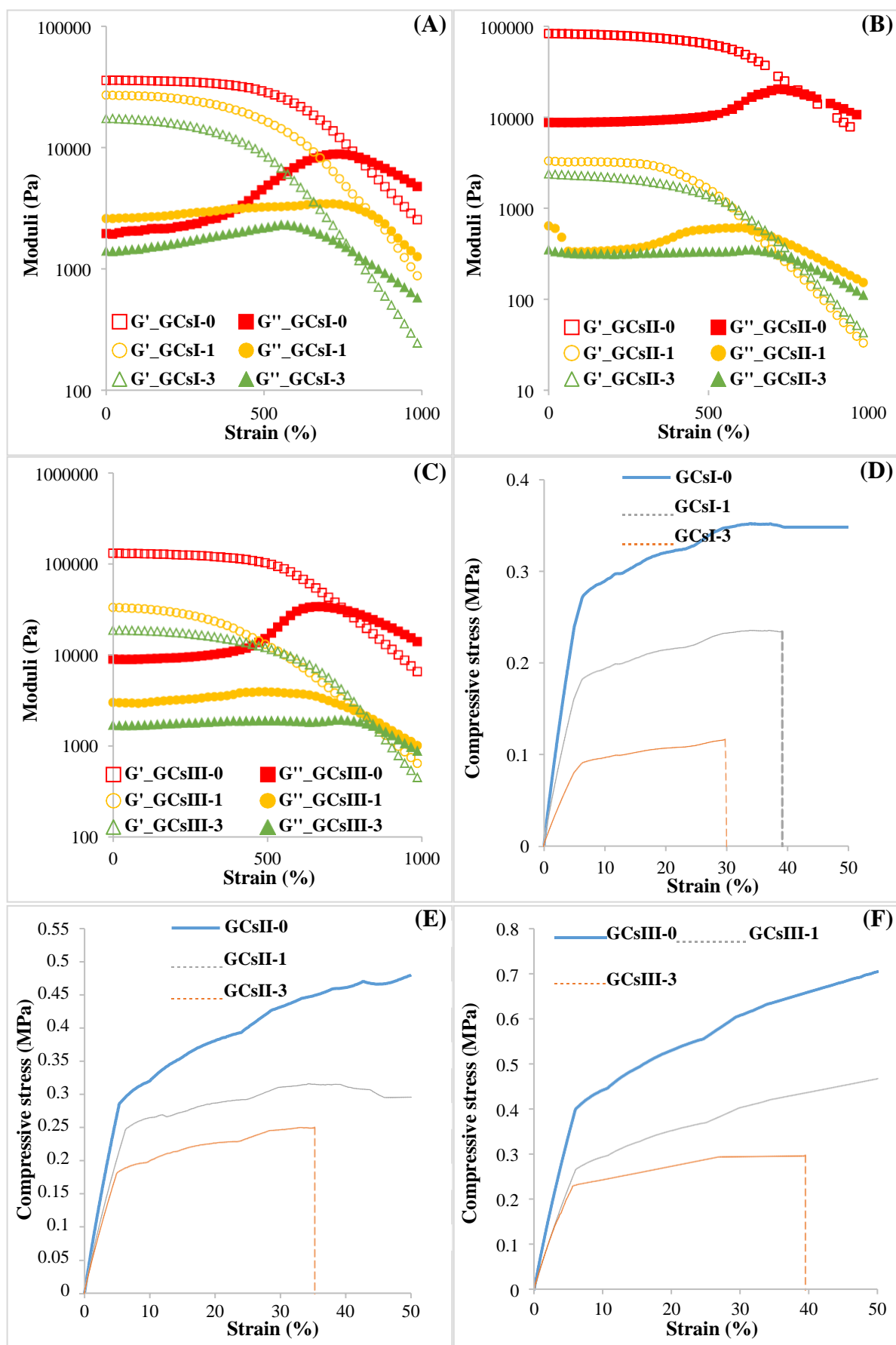
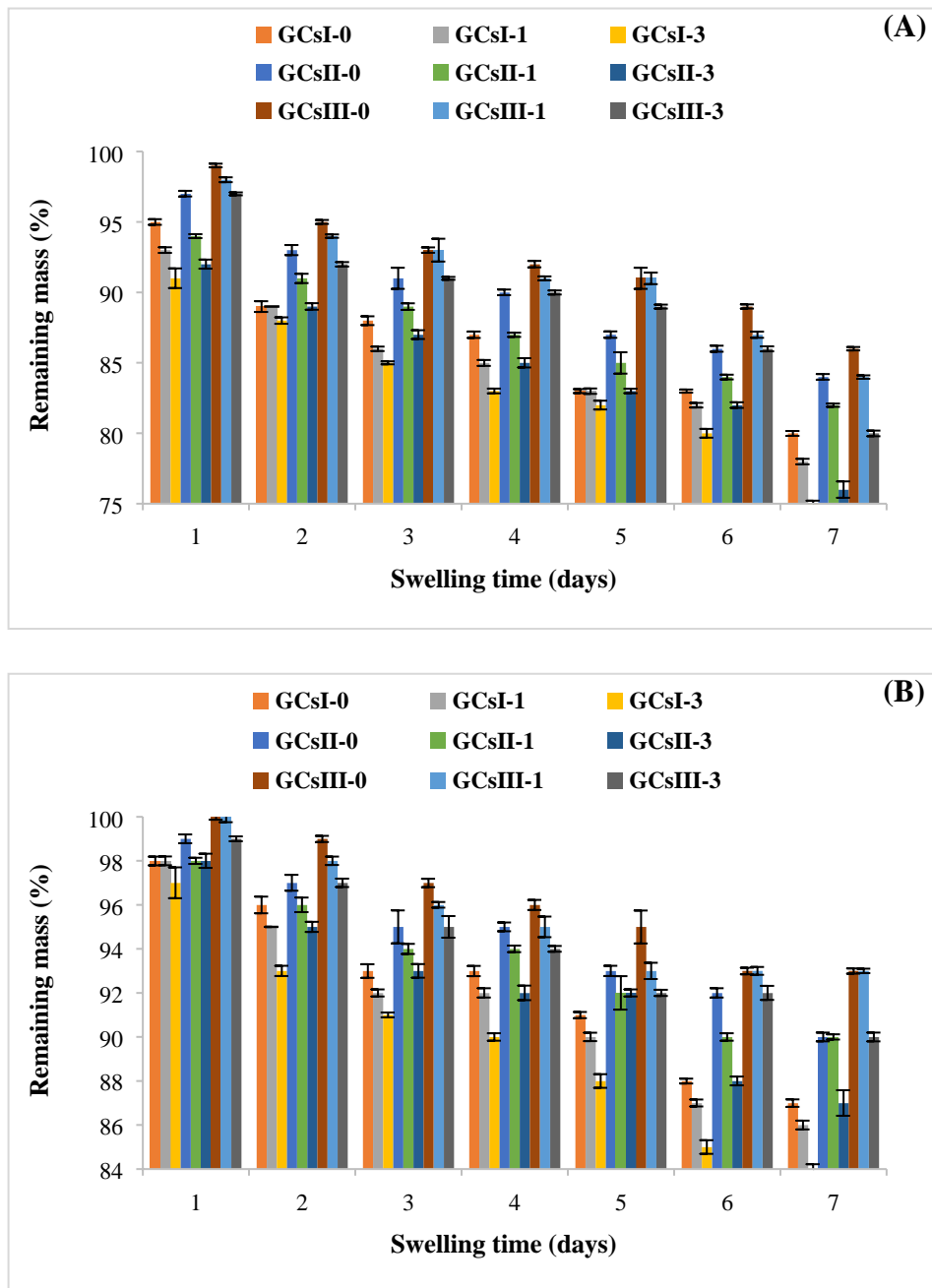


Fig. 5



**Fig. 6**

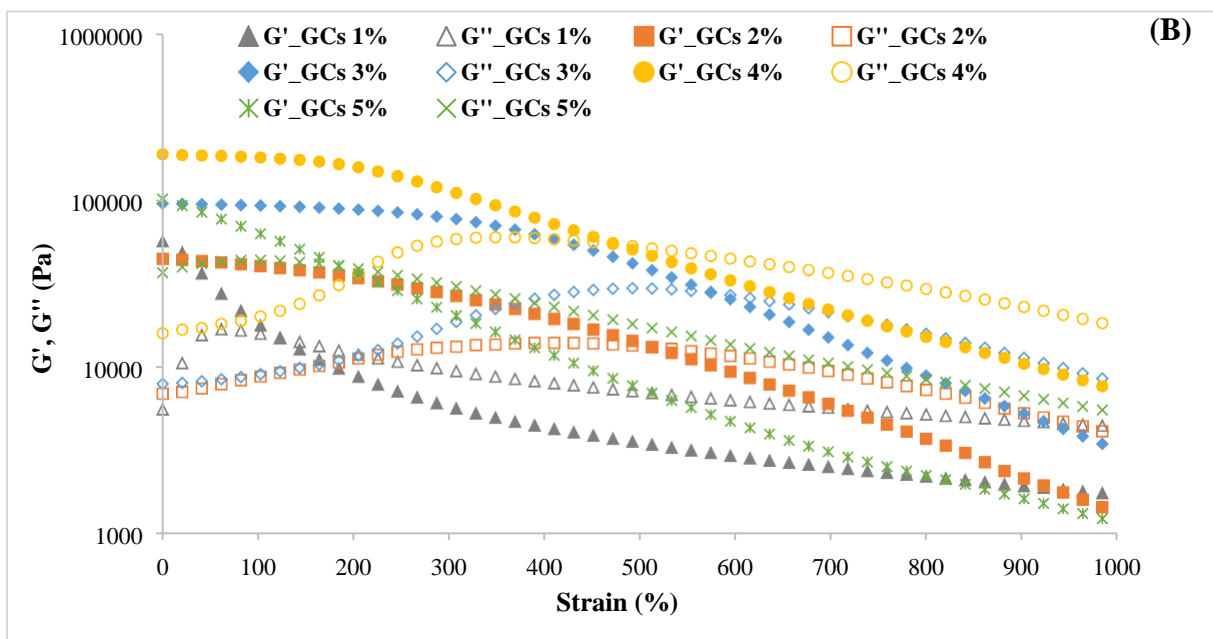
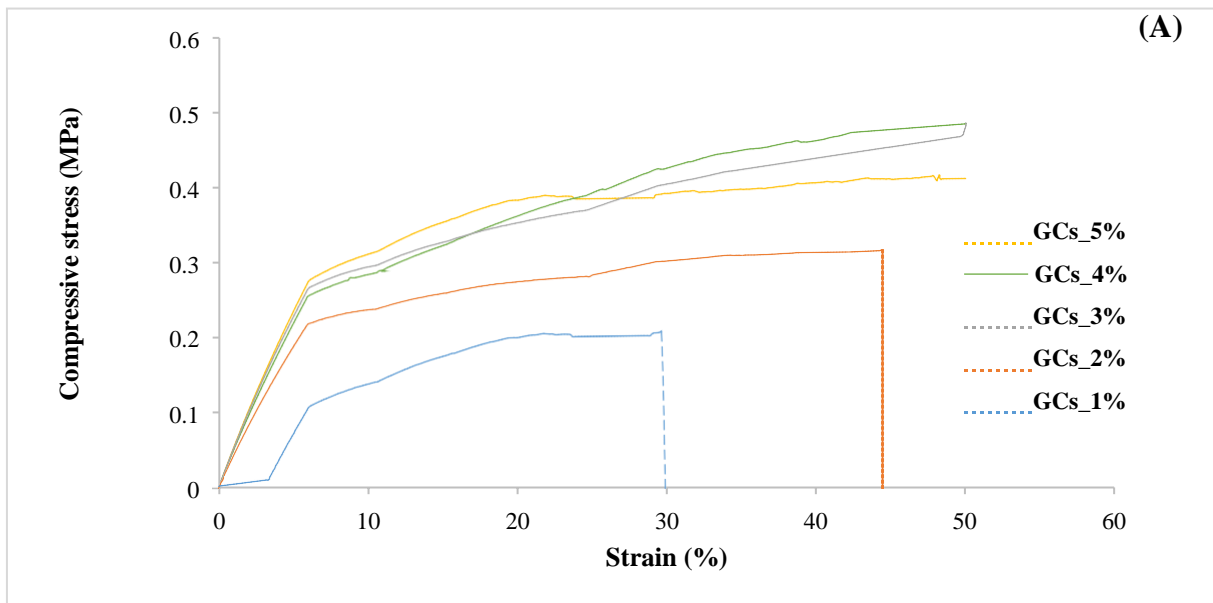
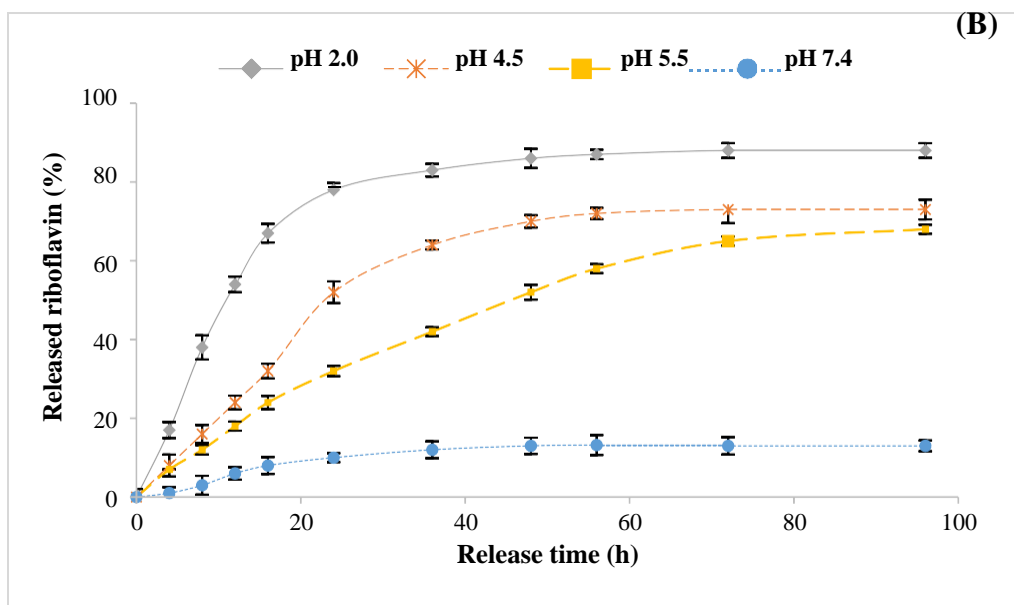
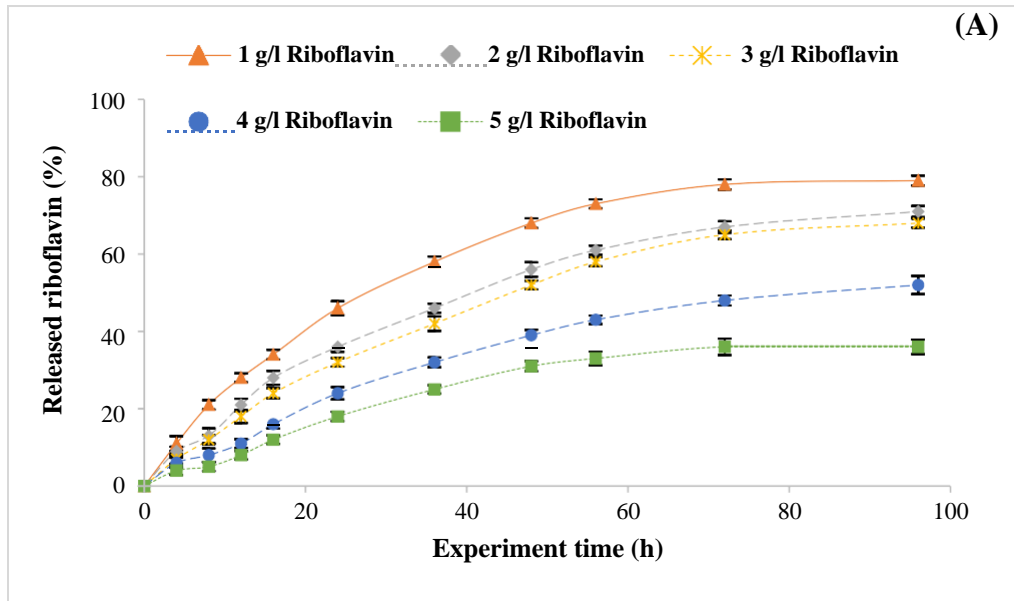




Fig. 7



**Fig. S1**

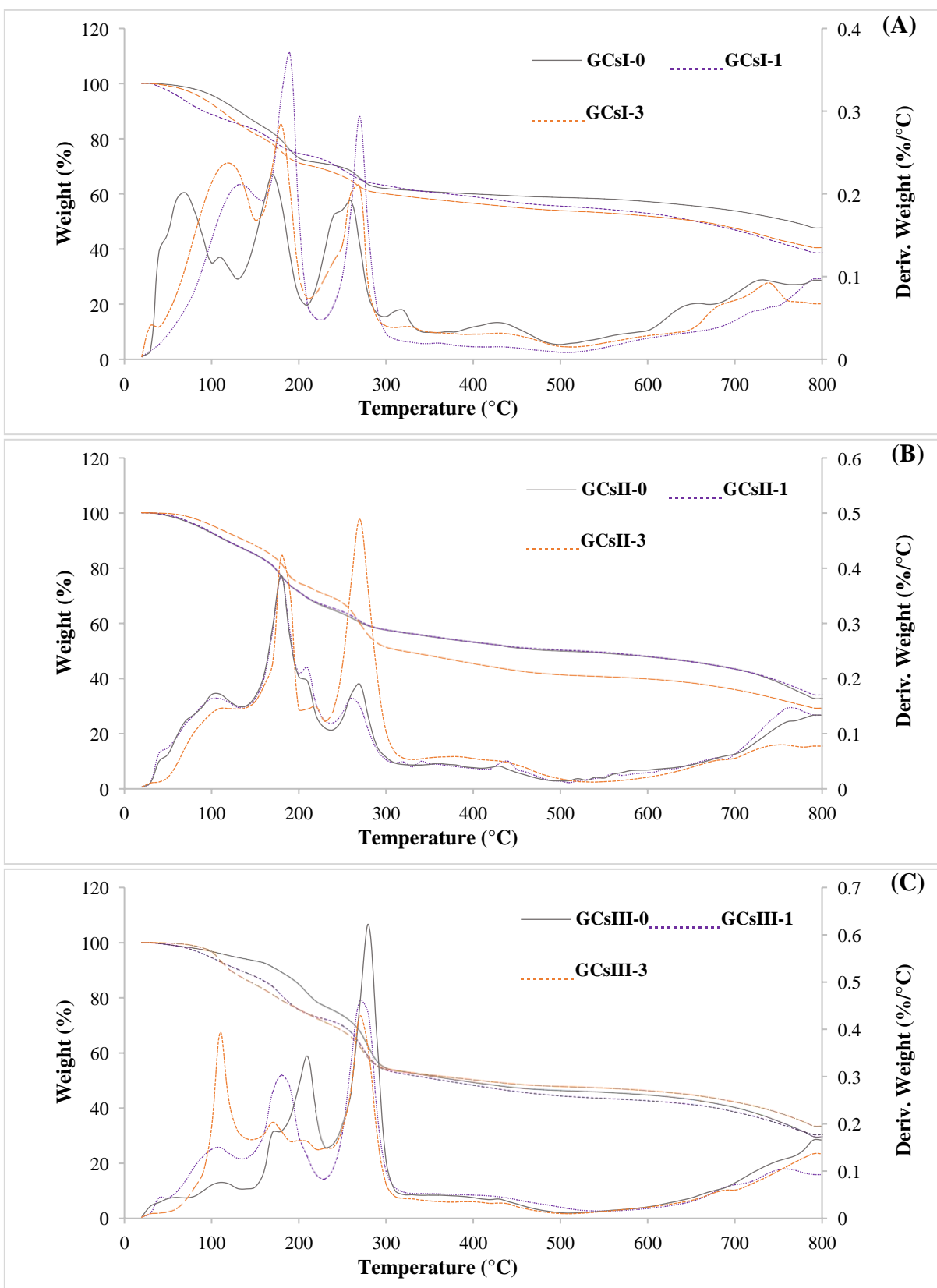
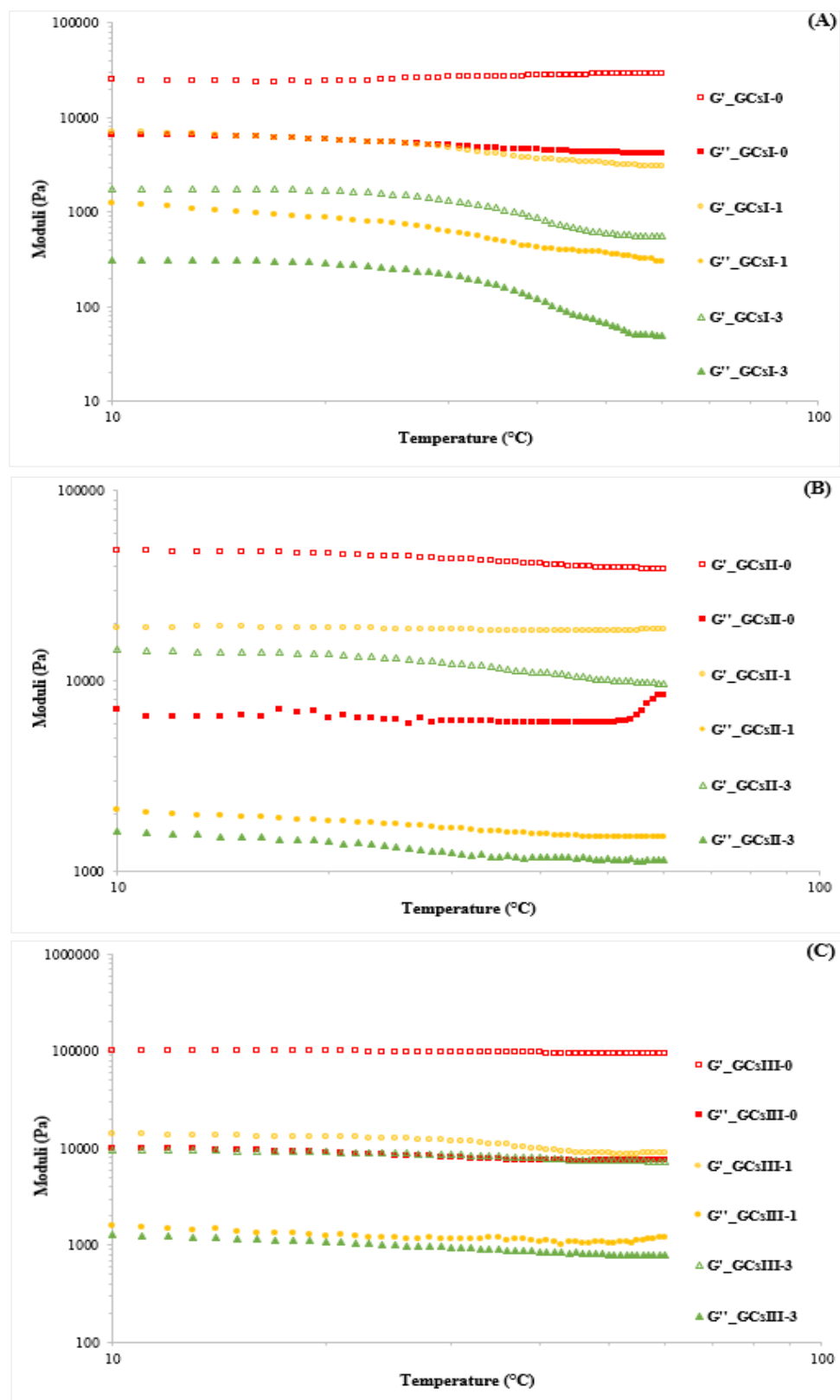


Fig. S2



**Table 1:** Moisture content (MC) and swelling ratio (SR) of different prepared Cs-based hydrogels.

Cs-based hydrogels	3% (w/v) Cs content					
	GCsI		GCsII		GCsIII	
	MC (%)	SR (g/g)	MC (%)	SR (g/g)	MC (%)	SR (g/g)
<b>GCs-0</b>	82.36±0.72 <sup>aB</sup>	13.59±0.45 <sup>aA</sup>	81.34±0.22 <sup>aB</sup>	16.57±1.04 <sup>aB</sup>	79.90±0.09 <sup>aA</sup>	18.10±0.47 <sup>aC</sup>
<b>GCs-1</b>	86.52±1.35 <sup>bC</sup>	14.92±0.32 <sup>bA</sup>	81.78±0.11 <sup>aB</sup>	18.93±0.32 <sup>bB</sup>	80.26±0.04 <sup>bA</sup>	22.21±0.53 <sup>bC</sup>
<b>GCs-3</b>	89.08±0.69 <sup>cC</sup>	16.38±0.27 <sup>cA</sup>	83.20±0.06 <sup>bB</sup>	22.86±0.78 <sup>cB</sup>	81.83±0.08 <sup>cA</sup>	26.24±0.93 <sup>cC</sup>

Different letters (a-c) in the same column are significantly different as determined by ANOVA test ( $p < 0.05$ ).

Different letters (A-C) in the same line indicated significant differences within hydrogels based on Cs with different AD ( $p < 0.05$ ).

**Table 2:** Cs-based hydrogels degradation temperatures (**Td**: onset temperature of degradation, **Tmax**: maximum degradation temperature and **Tf**: temperature of the end of degradation), the weight loss ( $\Delta w$ ) and the residue (**R**).

Parameters	GCsI			GCsII			GCsIII			
	GCsI-0	GCsI-1	GCsI-3	GCsII-0	GCsII-1	GCsII-3	GCsIII-0	GCsIII-1	GCsIII-3	
<b>rnase I</b>	$\Delta W$ (%)	11.46	15.69	18.93	8.66	12.14	12.73	5.65	10.30	14.75
	<b>Td</b> (°C)	27.32	33.30	40.93	30.03	37.75	42.75	36.39	41.71	45.47
	<b>Tmax</b> (°C)	114.47	104.49	66.35	118.10	109.02	104.49	133.54	109.93	106.35
	<b>Tf</b> (°C)	147.16	133.54	129.00	153.51	134.45	129.91	158.96	135.35	130.81
<b>rnase II</b>	$\Delta W$ (%)	13.30	14.43	10.72	20.95	21.24	22.50	17.18	18.19	14.04
	<b>Td</b> (°C)	147.16	133.54	129.00	153.51	134.45	129.91	158.96	135.35	130.81
	<b>Tmax</b> (°C)	184.38	176.21	169.85	188.01	179.84	172.58	208.89	179.84	175.30
	<b>Tf</b> (°C)	227.05	210.71	207.08	235.22	229.77	226.13	235.22	231.59	227.05
<b>Phase III</b>	$\Delta W$ (%)	12.42	16.59	18.63	29.34	15.52	15.29	28.77	29.72	23.29
	<b>Td</b> (°C)	227.05	210.71	207.08	235.22	229.77	226.13	235.22	231.59	227.05
	<b>Tmax</b> (°C)	268.81	266.09	261.55	269.72	267.00	262.46	279.71	274.26	273.35
	<b>Tf</b> (°C)	511.22	507.58	502.14	537.54	508.49	502.14	547.53	510.31	509.40
<b>R</b> (%)	38.68	40.53	47.69	29.58	33.05	34.34	29.88	30.59	33.70	

**Table 3:** Riboflavin entrapment efficiency (EE) and loading capacity (LC) of CsIII-0 based hydrogel, at a concentration of 3% (w/v).

Riboflavin concentration (g/l)	EE (%)	LC (%)
1	75.58 ± 0.61 <sup>c</sup>	23.51 ± 1.26 <sup>a</sup>
2	80.64 ± 1.59 <sup>d</sup>	31.14 ± 0.94 <sup>b</sup>
3	84.54 ± 1.35 <sup>e</sup>	36.57 ± 1.45 <sup>c</sup>
4	66.28 ± 0.52 <sup>b</sup>	37.19 ± 0.62 <sup>c</sup>
5	53.27 ± 1.72 <sup>a</sup>	37.81 ± 1.32 <sup>c</sup>

Different letters (a-e) in the same column are significantly different as determined by ANOVA test ( $p < 0.05$ ).

**Table S1:** Blue crab chitosan (Cs) nomenclature and respective acetylation degrees (AD) and average molecular weights ( $\text{g mol}^{-1}$ ).

average molecular weights ( $\text{g mol}^{-1}$ ).				
Cs	—	17	13	8
<b>Cellulase digestion reaction-time (h)</b>	0	CsI-0	CsII-0	CsIII-0
	1	CsI-1	CsII-1	CsIII-1
	3	CsI-3	CsII-3	CsIII-3
Cs	—	17	13	8
<b>Digestion reaction-time (h)</b>	0	125 600	118 900	115 000
	1	17 800	59 270	78 430
	3	10 440	18 540	16 040

**Table S2:** Different blue crab chitosan-based hydrogels (GCs) feed compositions and respective nomenclature.

<b>Cs-based hydrogels</b>	<b>3% (w/v) Cs content</b>		
	<b>CsI</b>	<b>CsII</b>	<b>CsIII</b>
<b>Cs-0</b>	GCsI-0	GCsII-0	GCsIII-0
<b>Cs-1</b>	GCsI-1	GCsII-1	GCsIII-1
<b>Cs-3</b>	GCsI-3	GCsII-3	GCsIII-3